AD-A190 877 POLARIMETRIC ISAR IMAGING USING EITHER MEASURED OF CALCULATED TRANSIENT SIGNATURES(U) OHIO STATE UNIV COLUMBUS ELECTROSCIENCE LAB G DURAL ET AL OCT 87 1/1

UNCLASSIFIED ESL-718048-6 F/G 17/9 NL

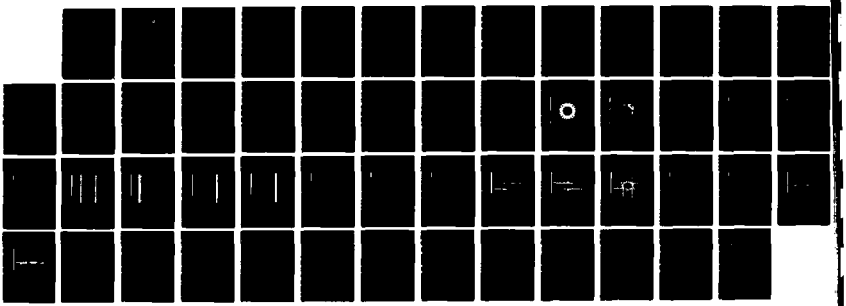

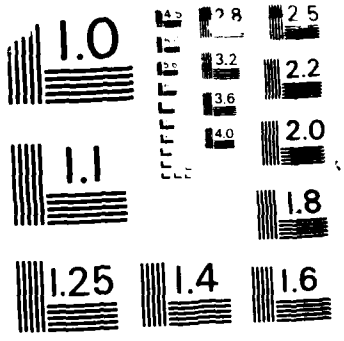

POLARIMETRIC ISAR IMAGING USING EITHER MEASURED OR CALCULATED TRANSIENT SIGNATURES

Gülbin Dural
Jonathan D. Young

The Ohio State University
ElectroScience Laboratory
Department of Electrical Engineering
Columbus, Ohio 43212

"Original contains color plates: All DTIC reproductions will be in black and white"

Technical Report No. 718048-6
Contract No. N00014-86-K-0202
October 1987

Department of the Navy
Office of Naval Research
800 N. Quincy Street
Arlington, Virginia 22217

NOTICES

When Government drawings, specifications, or other data are used for any purpose other than in connection with a definitely related Government procurement operation, the United States Government thereby incurs no responsibility nor any obligation whatsoever, and the fact that the Government may have formulated, furnished, or in any way supplied the said drawings, specifications, or other data, is not to be regarded by implication or otherwise as in any manner licensing the holder or any other person or corporation, or conveying any rights or permission to manufacture, use, or sell any patented invention that may in any way be related thereto.

50272-101

REPORT DOCUMENTATION PAGE	1. REPORT NO.	2.	3. Recipient's Accession No

4. Title and Subtitle

POLARIMETRIC ISAR IMAGING USING EITHER MEASURED OR CALCULATED TRANSIENT SIGNATURES

5. Report Date
October 1987

6.

7. Author(s)
G. Dural and J.D. Young

8. Performing Organization Rept. No
718048-6

9. Performing Organization Name and Address
The Ohio State University ElectroScience Laboratory
1320 Kinnear Road
Columbus, Ohio 43212

10. Project/Task/Work Unit No

11. Contract(C) or Grant(G) No
(C) N00014-86-K-0202
(G)

12. Sponsoring Organization Name and Address
Department of the Navy
Office of Naval Research
800 N. Quincy Street
Arlington, VA 22217

13. Type of Report & Period Covered
Technical

14.

15. Supplementary Notes

16. Abstract (Limit: 200 words)

An approximation to generate ISAR images from electromagnetic scattering data is illustrated. An imaging algorithm which combines 1-D filtered time domain signals with aspect angle information is used to substitute for the 2-D Fourier transform. Polarimetric scattering characteristics of the targets are investigated. Images of the targets with different linear polarizations are generated and compared. Different sets of colors are assigned to different polarizations to illustrate the polarization dependence of the targets. Both measured and simulated data based on UTD are used with the same frequency window. Different scattering mechanisms observed on the measured and calculated images are discussed. Frequency scaling techniques are applied to combine measured data to widen the bandwidth. The work has concentrated on both geometrically simple and more complicated targets. Polarization is shown to be a useful tool in target identification with imaging.

17. Document Analysis a. Descriptors

b. Identifiers/Open-Ended Terms

c. COSATI Field/Group

18. Availability Statement
Approved for public release; distribution is unlimited.

19. Security Class (This Report)
Unclassified

20. Security Class (This Page)
Unclassified

21. No. of Pages
48

22. Price

(See ANSI-Z39.18) See Instructions on Reverse

OPTIONAL FORM 272 (4-7
(Formerly NTIS-35)
Department of Commerce

Contents

List of Figures

1. INTRODUCTION

Electromagnetic fields incident on a scattering object induce electric and/or magnetic currents which radiate to produce scattered fields. An image is a synthetic picture of an object generated from electromagnetic scattering data rather than the direct observation of the target [1]. The IEEE definition for image is "a spatial distribution of a physical property such as radiation, electric charge, conductivity or reflectivity, mapped from another distribution of either the same or another property" [2]. An image permits human visual recognition and identification of the object which may also carry detailed information about the scattering characteristics of the object. Imaging techniques have a large variety of applications such as target recognition and identification, diagnostic methods, acoustic imaging for medical diagnosis, seismic imaging and many others.

Most of the image reconstruction techniques are based on the fact that a two-dimensional (2-D) image of an object, which can be represented by a 2-D distribution of scattering centers, and its 2-D frequency spectra are Fourier transform pairs [3,4,5]. Therefore the image of a 2-D object can simply be generated by inverse Fourier transforming the 2-D frequency domain data. The imaging algorithm used in this paper utilizes 1-D filtered time domain signals together with aspect angle information and replaces the conventional 2-D Fourier transform.

The scattering characteristics of most targets are polarization dependent which makes the images polarization dependent also. Hence, polarization is an important parameter for target identification by imaging. In this report, images of both geometrically simple (like sphere, ellipsoid, square plate) and complicated (like an aircraft) targets using different polarizations are generated and compared. Two different sets of colors assigned to vertically (VP) and horizontally (HP) polarized images in order to display the polarization dependence of the images.

Scattering measurements of several targets were made using The Ohio State University Compact Radar Cross Section Measurement Range [6]. Most of the measured data span the range 2-18 GHz. For some of the targets, the frequency scaling technique permitted data between 0.01-18 GHz to be obtained. Calculated data were generated using approximations based on uniform asymptotic techniques in terms of the Geometrical Theory of Diffraction (GTD) [7]. The same frequency range was used for measured and calculated data in order to directly compare measured and calculated images.

Chapter 2 covers the basic theory related to the image reconstruction. Relationship between the frequency spectra and the image, imaging algorithm used and the sampling criteria are all discussed in this chapter. Chapter 3 covers the applications of the theory discussed in Chapter 2. Also, measurement and data processing techniques used are discussed and some results using either measured or simulated data with different polarizations are illustrated. Conclusions drawn from the research are discussed in Chapter 4.

2. BASIC THEORY

The image of an object can be characterized by a 2-D distribution of the scattering centers which is related to the 2-D frequency spectra by a 2-D inverse Fourier transform relationship. This relationship has been derived and discussed in Section 2.1. Section 2.2 covers the imaging algorithm. Limitations on the images due to space and frequency sampling criterion are discussed in section 2.3.

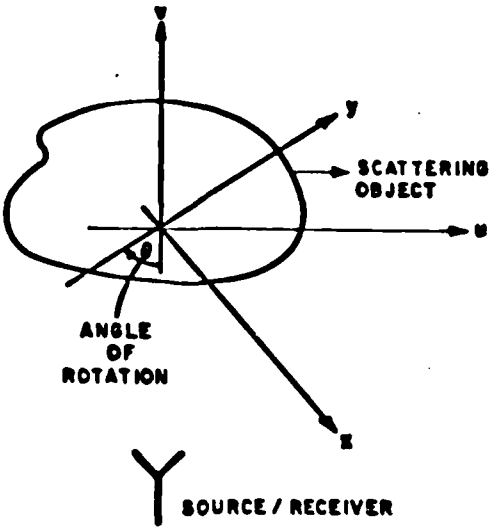

Figure 2.1: Imaging geometry for a two-dimensional object.

2.1 Image Reconstruction Using 2-D Frequency Spectra

To understand how an image is generated using either measured or simulated data, assume a rotating object which is uniformly illuminated by a stationary transmitter as shown in Figure 2.1. The object is rotated through an angle θ and scattered signals are recorded as a function of frequency and aspect angle. Also assume that the source is monochromatic (CW) with a frequency f. The objective is to obtain a 2-D image of this object in the cross-sectional plane. The cross-section of the object is represented by a 2-D distribution of scattering centers, $g(x, y)$, which is denoted as the "reflectivity density function" [4,5]. Assume y and x are the fixed and u and v are the rotated down and cross range coordinates, respectively. For a fixed θ, the total received signal will be the summation of the contributions of all the scattering centers; i.e., the integral of $g(x, y)$ over u and v assuming that for a fixed range, all scattered fields are in phase. A phase factor of e^{-j2kv} must be supplied to account for the phase delay along the down-range.

$$G(\theta) = \int_{-\infty}^{\infty}\int_{-\infty}^{\infty} g_\theta(u,v)e^{-j2kv}du\ \ dv$$
$$= \int_{-\infty}^{\infty}\int_{-\infty}^{\infty} g_\theta(u,v)e^{-j4\pi v/\lambda}du\ \ dv, \tag{2.1}$$

where k is the wave number and $g_\theta(u,v)$ is the reflectivity density function for a particular aspect θ.

Rotated and fixed coordinates are related as,

$$\begin{bmatrix} x \\ y \end{bmatrix} = \begin{bmatrix} \cos\theta & -\sin\theta \\ \sin\theta & \cos\theta \end{bmatrix} \begin{bmatrix} u \\ v \end{bmatrix} \tag{2.2a}$$

and

$$\begin{bmatrix} u \\ v \end{bmatrix} = \begin{bmatrix} \cos\theta & \sin\theta \\ -\sin\theta & \cos\theta \end{bmatrix} \begin{bmatrix} x \\ y \end{bmatrix} \tag{2.2b}$$

Using Equation (2.2b) in Equation (2.1), one obtains

$$G(\theta) = \int_{-\infty}^{\infty}\int_{-\infty}^{\infty} g(x,y)e^{-j\frac{4\pi}{\lambda}(y\cos\theta - x\sin\theta)}dxdy, \tag{2.3}$$

and defining the new variables f_x and f_y as,

$$f_x \triangleq -\frac{2\sin\theta}{\lambda}, \tag{2.4a}$$

$$f_y \triangleq \frac{2\cos\theta}{\lambda}. \tag{2.4b}$$

Equation (2.3) becomes,

$$G(f_x,f_y) = \int_{-\infty}^{\infty}\int_{-\infty}^{\infty} g(x,y)e^{-j2\pi(f_x x + f_y y)}dxdy, \tag{2.5}$$

which is a Fourier transform relationship. Therefore, $g(x,y)$ can be reconstructed by inverse Fourier transforming $G(f_x,f_y)$,

$$g(x,y) \overset{F.T.}{\Longleftrightarrow} G(f_x,f_y), \tag{2.6}$$

or

$$g(x,y) = \int_{-\infty}^{\infty}\int_{-\infty}^{\infty} G(f_x,f_y)e^{j2\pi(f_x x + f_y y)}df_x df_y. \tag{2.7}$$

With previous assumptions, $g(x,y)$ of Equation (2.7) corresponds to a monochromatic wave of frequency f. For a band of frequencies, the resultant $g(x,y)$ must be the summation of the contributions of each frequency component.

$$g(x,y) = \sum_{i=1}^{n} F^{-1}\left\{G(f_{x_i}, f_{y_i})\right\}, \tag{2.8}$$

or, using the linearity property of the Fourier transform,

$$g(x,y) = F^{-1}\left\{\sum_{i=1}^{n} G(f_{x_i}, f_{y_i})\right\}, \tag{2.9}$$

which is a 2-D Fourier transform relationship. Therefore, one can recover $g(x,y)$ simply by inverse Fourier transforming the 2-D frequency spectra.

2.2 Imaging Algorithm

In Section 2.1 it was shown that the image of an object and its 2-D frequency spectra are Fourier transform pairs. Hence, the image of a target can be reconstructed by simply inverse Fourier transforming the 2-D frequency domain data. On the other hand, measured data are usually sampled on a polar raster rather than a cartesian one and need to be converted to a cartesian raster in order to get compatible data for the 2-D FFT algorithms. Conversion from polar to rectangular coordinates requires interpolation of the data points which makes quality of the final image very dependent on the method of interpolation and also increases the computation time. Also, density of the polar data becomes sparser as one gets farther away from the center, so interpolation error becomes greater for the higher frequency components which results in some image degradation.

An alternative algorithm which is described in the following sections requires no interpolation and uses 1-D FFT and an additional algorithm making use of the well known "Fourier Slice Theorem" (or "Projection Slice Theorem") and back-projection techniques [8,9,10,3] can be used to improve the quality of the images.

2.2.1 Fourier Slice Theorem

Let $h(x,y)$ be a 2-D function and assume its 2-D Fourier transform exists.

$$h(x,y) \overset{FT}{\Longleftrightarrow} H(f_x, f_y), \tag{2.10}$$

u and v are the rotated coordinates as defined in Equations (2.2a) and (2.2b). Let $p_\theta(u)$ be the projection of $h(u,v)$ at angle θ, defined by

$$P_\theta(u) = \int_{-\infty}^{\infty} P(x,y)dv,$$

$$= \int_{-\infty}^{\infty} P(u\cos\theta - v\sin\theta, u\sin\theta + v\cos\theta)dv, \tag{2.11}$$

and assume its Fourier transform, $P_\theta(\omega)$ exists.

$$P_\theta(\omega) = FT\{p_\theta(u)\} = \int_{-\infty}^{\infty} p_\theta(u)e^{-j\omega u}du$$

$$= \int_{-\infty}^{\infty}\int_{-\infty}^{\infty} h(u\cos\theta - v\sin\theta, u\sin\theta + v\cos\theta)e^{-j\omega u}dudv. \tag{2.12}$$

Transforming back to the unrotated coordinate system,

$$P_\theta = \int_{-\infty}^{\infty}\int_{-\infty}^{\infty} h(x,y)e^{-j\omega(x\cos\theta + y\sin\theta)}dxdy, = H(\omega\cos\theta, \cos\theta). \tag{2.13}$$

or

$$P_\theta(f) = H(f\cos\theta, f\sin\theta). \tag{2.14}$$

Hence, if the (u,v) pair is rotated by an angle θ, the Fourier transform of the projection is equal to the 2-D Fourier transform of the object along a line rotated by θ. This result leads to the "Fourier Slice Theorem" which is stated as [9,10]: "the Fourier transform of a parallel projection of an image $h(x,y)$ taken at an angle θ gives a slice of the 2-D transform $H(f_x, f_y)$ subtending an angle θ with the u axis." In other words, the Fourier transform of $P_\theta(u)$ gives the values of $h(f_x, f_y)$ along the line f in Figure 2.2.

The above theorem indicates that by taking projections of an image at angles $\theta_j (j = 1,2,\ldots,n)$ and Fourier transforming each of these projections, values of

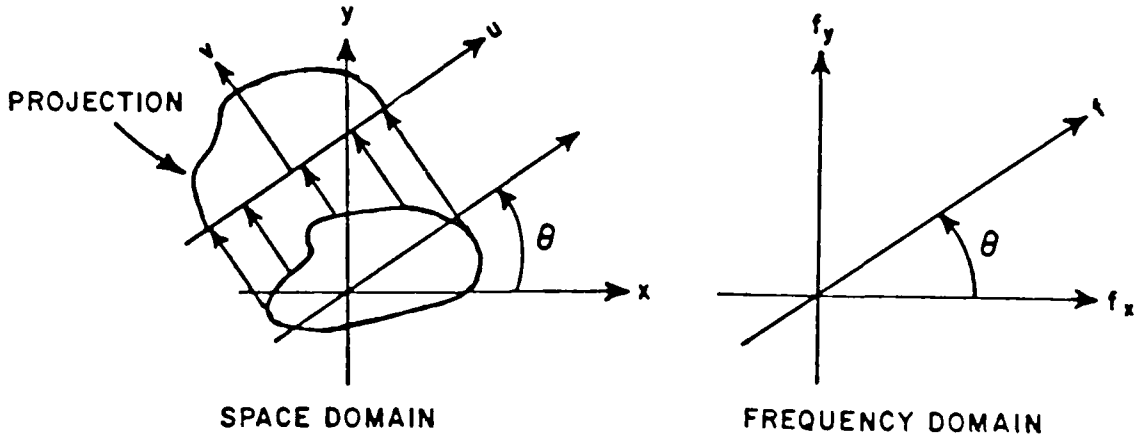

Figure 2.2: Projection of a 2-D function and the slice of its Fourier transform.

$H(f_x, f_y)$ can be determined along the radial lines shown in Figure 2.2. If $H(f_x, f_y)$ is known at a sufficiently large number of points on the (f_x, f_y) plane by taking a sufficiently large number of projections, then the 2-D image of the object can be reconstructed by inverse Fourier transform techniques.

2.2.2 Image Reconstruction

Recalling the formula for inverse Fourier transform,

$$h(x,y) = \int_{-\infty}^{\infty}\int_{-\infty}^{\infty} H(f_x, f_y) e^{j2\pi(f_x x + f_y y)} df_x df_y. \tag{2.15}$$

Defining a polar coordinate system (f, θ) by

$$f_x = f\cos\theta, \tag{2.16a}$$

$$f_y = f\sin\theta, \tag{2.16b}$$

and

$$du\ dv = f df d\theta, \tag{2.17}$$

one can represent the 2-D inverse Fourier transform of Equation (2.15) in a polar coordinate system. Where,

$$h(x,y) = \int_0^{2\pi} \int_0^{\infty} H(f,\theta) e^{j2\pi f(x\cos\theta + y\sin\theta)} f\, d\, f d\theta. \tag{2.18}$$

This integral can be split into two by considering $0 \leq \theta \leq \pi$ and $\pi < \theta \leq 2\pi$.

$$\begin{aligned} h(x,y) &= \int_0^{\pi} \int_0^{\infty} H(f,\theta) e^{j2\pi f(x\cos\theta + y\sin\theta)} f\ df\ d\theta \\ &+ \int_0^{\pi} \int_0^{\infty} H(f,\theta+\pi) e^{j2\pi f[x\cos(\theta+\pi) + y\sin(\theta+\pi)]} f\, d\, f d\theta, \end{aligned} \tag{2.19}$$

with the properties

$$H(f,\theta+\pi) = H(-f,\theta), \tag{2.20}$$

and

$$\cos(\theta+\pi) = -\cos\theta \tag{2.21a}$$

$$\sin(\theta+\pi) = -\sin\theta \tag{2.21b}$$

the integral of Equation (2.19) can be rewritten as,

$$\begin{aligned} h(x,y) &= \int_0^{\pi} \left[\int_{-\infty}^{\infty} H(f,\theta)|f| e^{j2\pi f(x\cos\theta + y\sin\theta)} df \right] d\theta \\ &= \int_0^{\pi} \left[\int_{-\infty}^{\infty} P_\theta |f| e^{j2\pi f t} df \right] d\theta. \end{aligned} \tag{2.22}$$

where $t = x\cos\theta + y\sin\theta$.

The inner integral represents a one-dimensional inverse Fourier transform of the product of the projection $p_\theta(f)$ and $|f|$. It thus corresponds to a filtered function. Summing the projections for each aspect angle, θ, an estimate for $h(x,y)$ can be

obtained. Substituting $g(x,y)$ for $h(x,y)$ in Equation (2.22), image reconstruction procedure can be summarized as follows: to every point (x,y) on the image plane, there corresponds a value of $t = x\cos\theta + y\sin\theta$ for a given value of θ and the filtered projection contributes to the reconstruction with its value of t. Making use of Equation (2.22), the new algorithm substitutes for the 2-D Fourier transform. Since it consists of only a 1-D Fourier transform plus an addition algorithm, it improves the quality of the images by avoiding the errors due to interpolation of the data points.

2.3 Limitations

From a practical point of view, it is not possible to have either a continuous frequency spectra or infinite aspect angles around the target. Therefore, the quality of the images produced also depends on the sampling rates of both frequency and aspect. On the other hand, in order to represent original continuous waveforms sampling rates must satisfy some criterion which will be discussed in the following sections.

2.3.1 Frequency Sampling Criteria

Discrete data sampling at the Nyquist rate for reconstruction of continuous waveforms is well known. From the sampling theorem [11,12]: "A time limited signal can be reproduced from its discrete values, if it is sampled over the complete frequency domain using the Nyquist rate." Where, f_s, the sampling rate should satisfy $f_s \leq 1/2T$ and signal is limited to time $\pm T$.

Then,

$$F(w) = \sum_{n=-\infty}^{\infty} F\left(\frac{n\pi}{T}\right) \frac{\sin(wT - n\pi)}{wT - n\pi}, \tag{2.23}$$

where samples are taken at $w = \frac{n\pi}{T}$, $-\infty < n < \infty$. To employ the sampling

theorem, the signal must be limited either in time or frequency. In our cases, targets are limited in space, or equivalently signals are limited in time. On the other hand, measured spectra is also frequency limited. Therefore, target images are expected to repeat in space.

Applications of sampling theorem for general N-dimensional cases has been studied by Fok [13] and the proposed frequency increment for the 2-D case is

$$\Delta f \leq \frac{c}{2(1+k)D}, \tag{2.24}$$

where, D is the maximum dimension of the object, C is the speed of light, and K is some safety factor.

2.3.2 Number of Projections Required

Given that one can only obtain a finite number of projections, N, what should the minimum value of N be? This depends to a great extent upon what is known a priori about the signal being reconstructed and how much detail we expect to learn about it. For example, if it is known a priori that an unknown signal is circularly symmetric (like scattering from a sphere), all its projections are identical and only one of them is necessary (and will be sufficient) to reconstruct $g(x,y)$. On the other hand, if absolutely nothing is known beforehand about $g(x,y)$ then an infinite number of projections will be required. To determine the minimum number of projections required, the angular increment which satisfies the Nyquist criterion is given by Mensa et al., [5]

$$\Delta\theta \leq \begin{cases} \frac{\lambda}{2D} & \lambda \ll 2D \\ sin^{-1}\frac{\lambda}{2D} & \lambda < 2D \\ \frac{\pi}{4} & \lambda \leq 2D. \end{cases} \tag{2.25}$$

3. APPLICATIONS

Up to this point, it has been shown how a 2-D image of a scattering target can be reconstructed in the spatial coordinates. On the other hand, scattering characteristics of most targets depend upon the polarization of the incident wave which requires one more dimension to be introduced, namely polarization, to make the images more identifiable. Early studies on polarization properties of the scattered waves have been carried on by Sinclair [14], Kennaugh [15] and Graves [16]. More recently, this property of scattered waves has been studied by Boerner et al. [17], and Kostinski et al. [18]. Also in most of the papers concentrated on the scattering from different geometries using different approximation techniques, such as GTD, one can find the formulation of the scattered field for that specific geometry for different polarizations.

In this report, images of some geometrically simple (sphere, tilted square plate, tilted ellipsoid) and more complicated (an aircraft) targets using either measured or simulated data were illustrated and analyzed. Section 3.1 briefly discusses measurement, approximations used to generate the simulated data and the data processing technique used for imaging. Section 3.2 illustrates the images produced including the discussions related to them.

3.1 Data Processing

Scattering measurements of several targets were made using The Ohio State University Compact Radar Cross Section Measurement Range [6]. Measured raw data are calculated using the calibration equations given by the same reference. After calibration and windowing processes the measured data become ready for the imaging process. Simulated data were generated using approximations based on uniform asymptotic techniques formulated in terms of the Geometrical Theory of

Diffraction (GTD) [7]. The imaging process can be summarized as follows:

1. Multiply the frequency domain data by the frequency (Equation (2.21)).
2. Inverse Fourier transform the filtered frequency data of Step 1.
3. Determine the image size which gives the size of the required time domain window.
4. Average a certain number of points on the time domain data (this number is determined by the time domain window of step 3) so that the image can be represented by a $n \times m$ matrix (100×100 is used).
5. Calculate the discrete coordinates on the image plane (a 100×100 matrix).
6. For each discrete point on the image plane, sum the contribution of each time domain response by rotating the time domain signals by θ.
7. If more than one polarization is required at the same time, go back to Step 5 for the new polarization.

A frequency range of 2-18 GHz has been used in most of the measurements. For square plate applications, two different scale models (ratio $< 8:1$) have been combined to widen the bandwidth to 0.01 to 18 GHz such that low frequency effects can also be observed. Simulated data spans the same frequency range in order to directly compare measured and calculated images.

Two linear polarizations, vertical (VP) and horizontal, are used to demonstrate the polarimetric scattering characteristics of the targets of interest. A Tekronix 429 color CRT display and hard copy unit are used to display the images. Two different sets of colors are assigned to encode the amplitude for each polarization. The computer programs CIMAG2 [22] and CLRPL (Appendix I) are used to generate the images and to plot them on the color display, respectively.

3.2 Results

The first target of interest is a sphere whose impulse response and images with different spatial windows are shown in Figures 3.3 through 3.5. Because it is a geometrically simple object, its scattering characteristics are well known [21,19], and also it is aspect and polarization independent. Hence, it is a useful introductory step to start imaging studies with a sphere to examine the imaging technique used and understand different features on the images. Figure 3.4 shows the image of the sphere with a 360° spatial window with 1° increments. The image of the same sphere with a 90° spatial window is shown in Figure 3.5. The frequency data used to generate these images range from 2 to 18 GHz in 10 MHz steps. Examining Figure 3.4, the red colored ring with the highest amplitude (or the red colored arc in Figure 3.5) corresponds to the outer radius of the sphere which is related to the specular response. Green colored rings outside the sphere with relatively lower amplitudes correspond to the higher order scattering mechanisms like creeping waves around the sphere. Three concentric circles inside the red one are related to the ripples around the specular in Figure 3.3. The same mechanisms discussed above can be observed in Figure 3.5. Since only a limited spatial window is used, the figure is not symmetric anymore. Therefore the delayed response related with the creeping waves which is represented by the green arc facing the red one can be more clearly identified in this figure.

Figures 3.7 through 3.14 belong to a 1 ft. tilted (45° from horizontal) square plate using either measured or simulated data with different spatial windows (90° and 360°) and linear polarizations (scattering mechanisms related to flat plate structures has been analyzed and discussed in detail by Sitka [20]). Frequency data spans a range of 0.01 - 18 GHz with 10 MHz steps, which was achieved by combining the frequency data belonging to 2 different scale modeled plates for the measured data. An impulse response waveform belonging to one of these combined data is shown

in Figure 3.6. First, comparing Figures 3.9 and 3.13, which are the images of the same plate with a spatial window of 90° using different linear polarizations, a stronger response is observed from the back edge in VP while the front edge is more dominant in HP, because the surface waves cannot propagate along the plate and contribute the scattering at the back edge in the HP case. A second order mechanism corresponding to the waves traveling along the plate is seen as a delayed response in Figure 3.9 (VP) which is coded by a yellow green line behind the back edge and it does not show up in Figure 3.13 because of the same reason discussed above. Response around 90° incidence (side edge on the right) is almost identical in both figures as expected. Strong responses at the corners are observed on both polarizations. Now, comparing Figures 3.9 and 3.10 or 3.13 and 3.14 a good agreement is observed between the measured and calculated images except that the second order mechanism observed on the measured image isn't seen in the calculated ones because simulated data are generated by a first order UTD approximation. The same discussions hold for Figures 3.7, 3.8, 3.11 and 3.12, the images with full 360° spatial window. One advantage of using a 90° spatial window is, that figures are not symmetric any more and it is easier to identify the delayed responses (it also requires far less data). In all of the square plate images discussed above, the increment for the aspect angle ($\Delta\theta$) used is 15° which does not satisfy the sampling criterion and causes some image degradation. Also, while combining some of the frequency data belonging to different scaled modeled plates, some alignment problems caused the combined data to be slightly blurred which produced some noise in the measured images too.

Figures 3.14 - 3.20 belong to a tilted ellipsoid with different elevations and two different linear polarizations. Frequency data spans a 1-12 GHz range with 10 MHz steps. The increment for the aspect angle is 30° which doesn't satisfy the sampling criteria. When Figures 3.14 - 3.16 or 3.17 - 3.20 are examined, the size of the figures

gets smaller as the tilt angle becomes larger because the projected area becomes smaller.

Figure 3.21 belongs to an image of a Boeing 707 aircraft with VP.

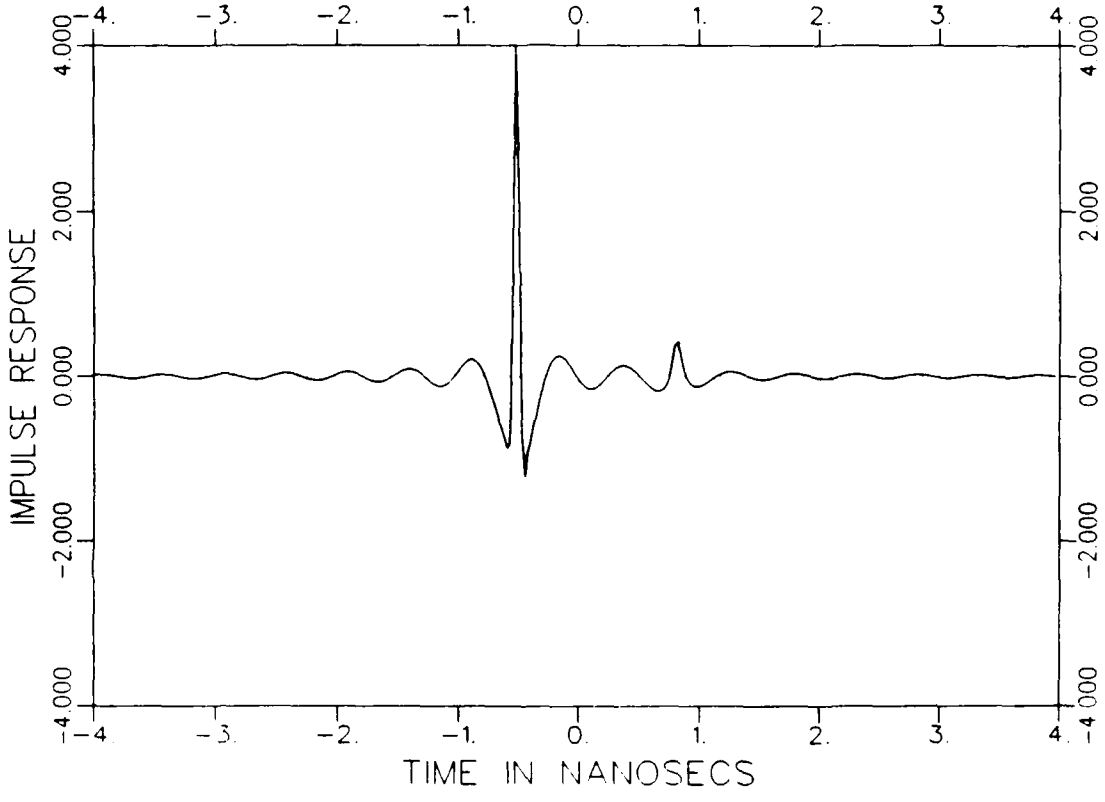

Figure 3.1: Impulse response of a 6 inch conducting sphere.

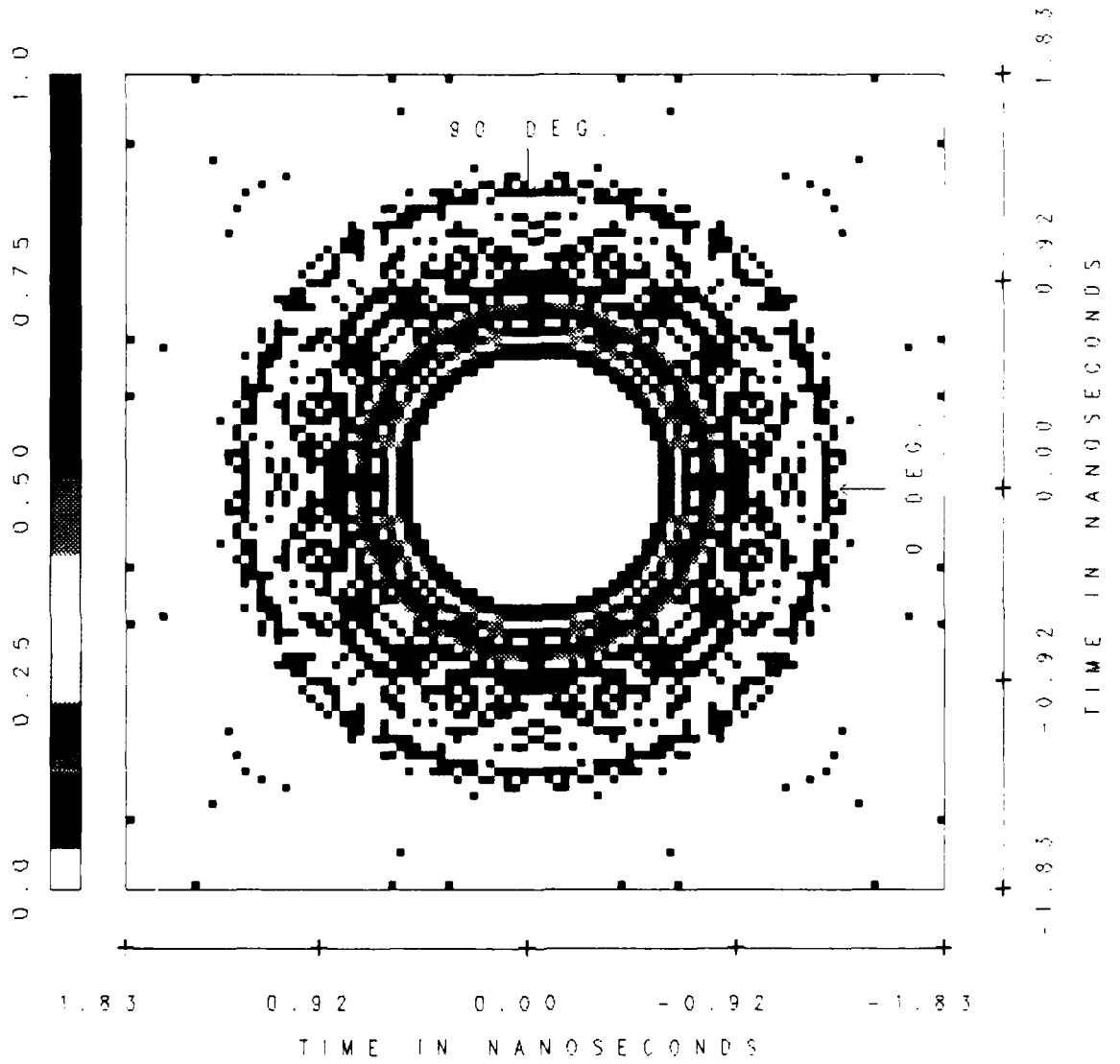

Figure 3.2: Image of a 6 inch conducting sphere.

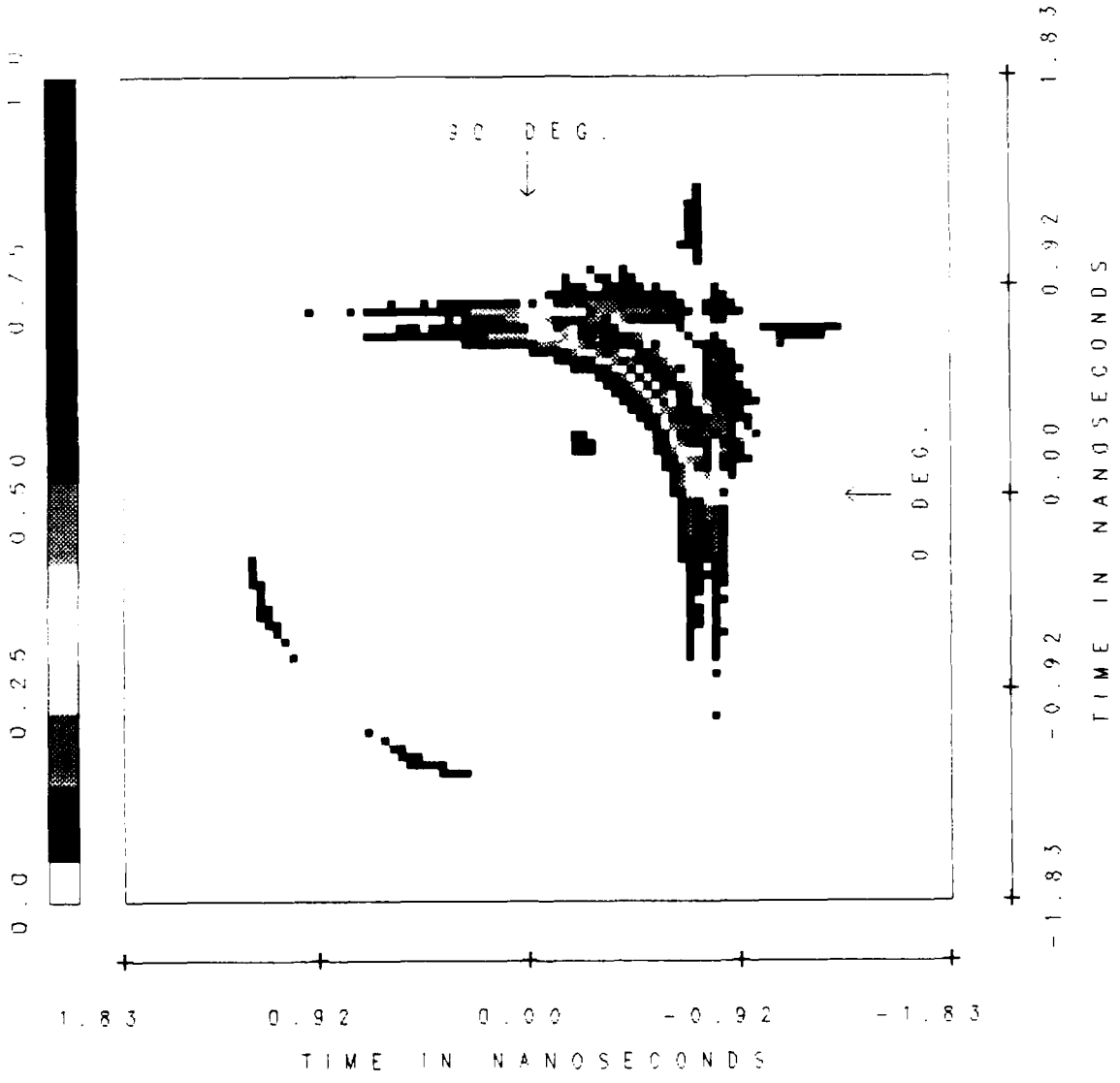

Figure 3.3: Image of a 6 inch conducting sphere with 90° spatial window.

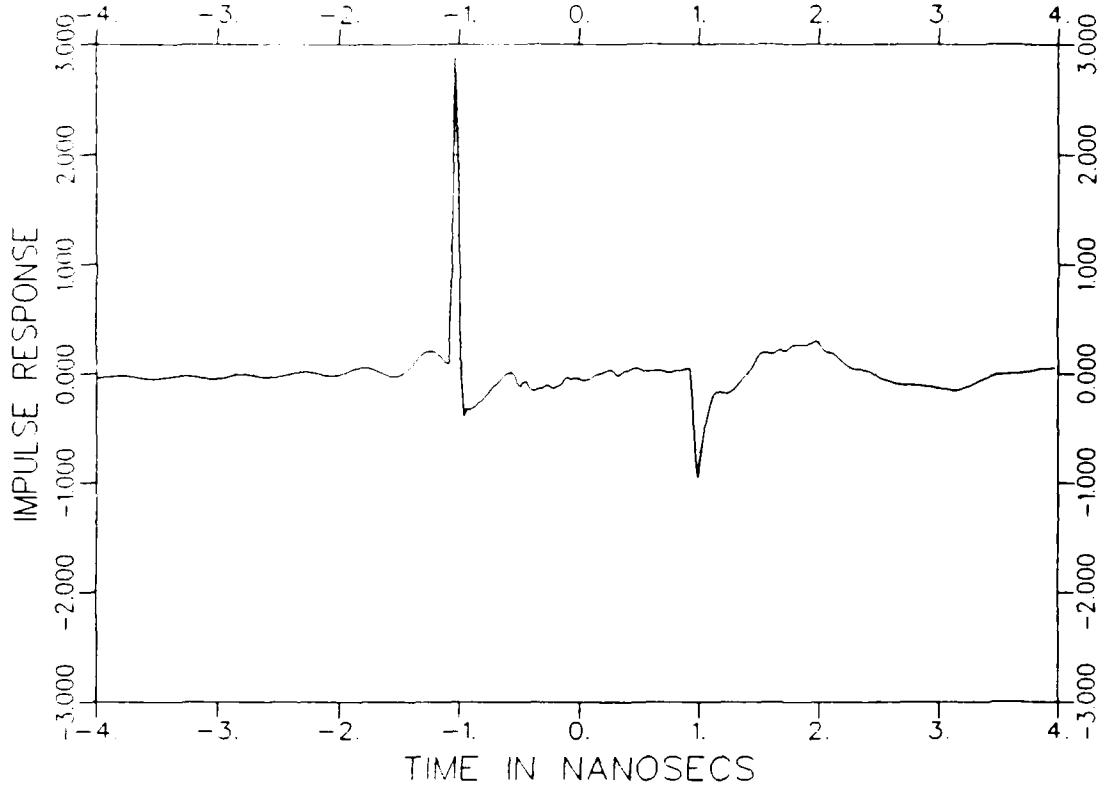

Figure 3.4: Impulse response of a 1 ft. tilted square plate. Elevation = 45°; aspect = 90°; frequency = 0.01 - 18 GHz. Result of combination of two differently scaled modeled plates (ratio 8:1) with 2-18 GHz, measured data.

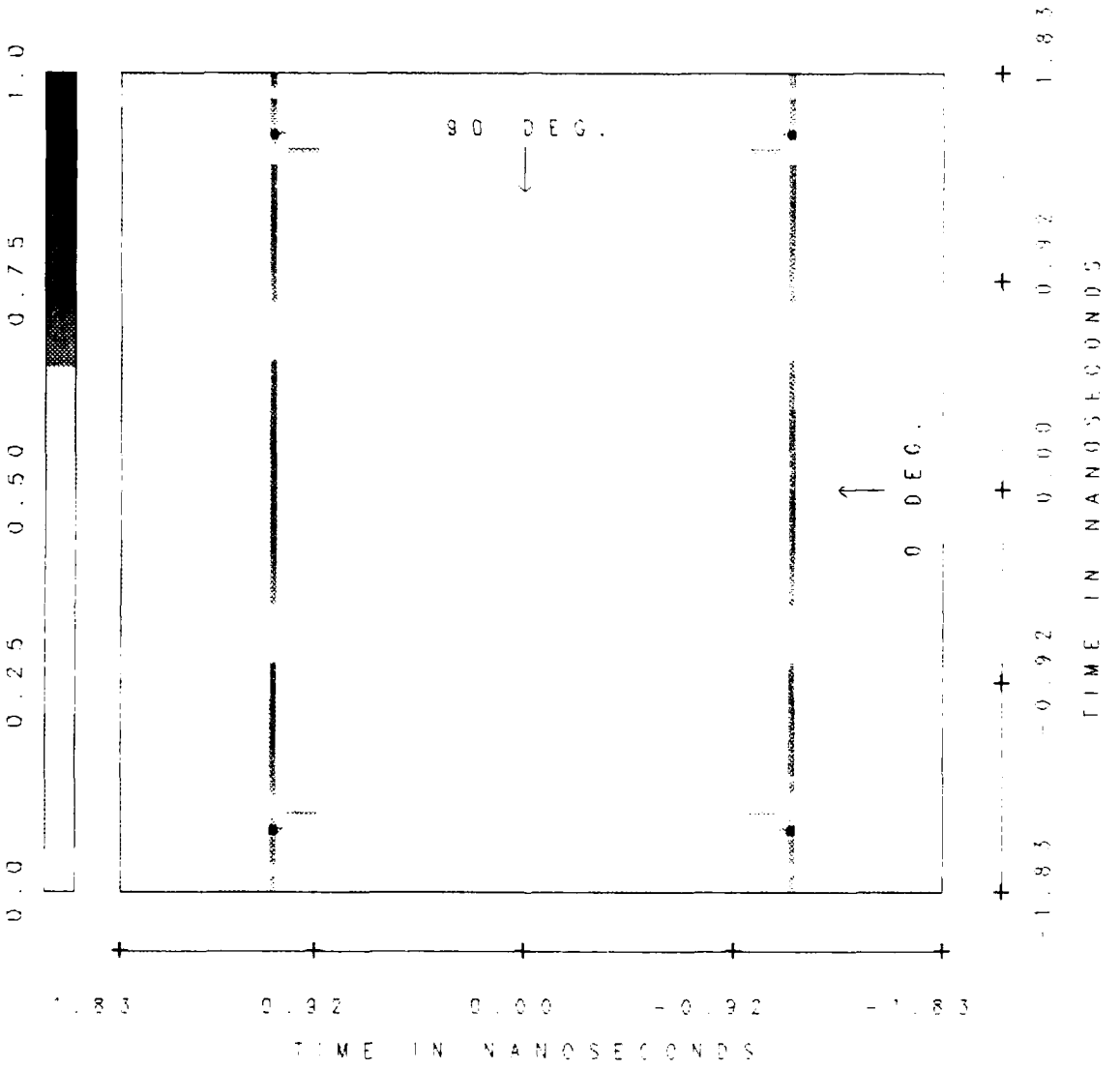

Figure 3.5: Image of a 1 ft. tilted square plate. Elevation = 45°; VP; measured data.

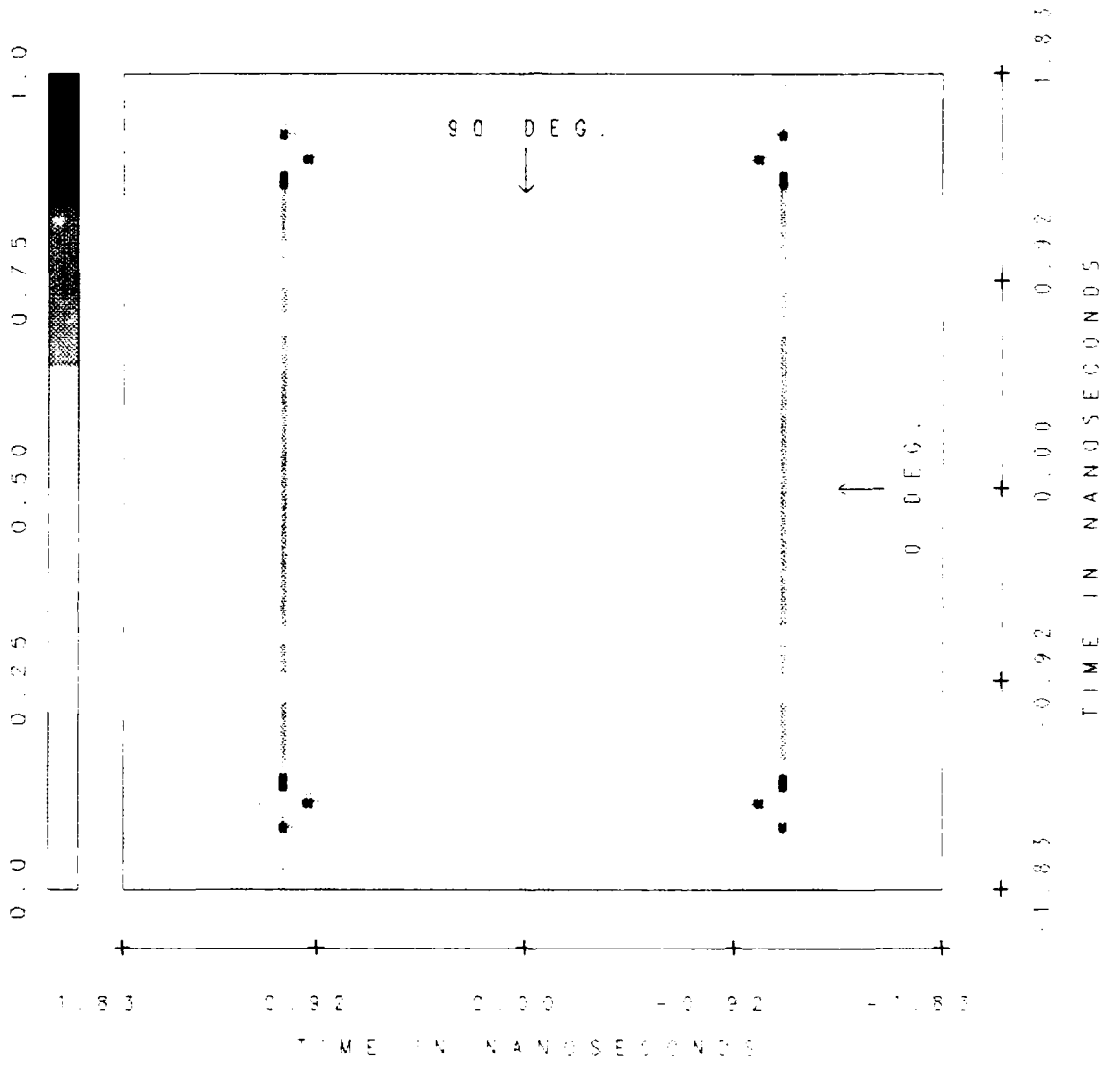

Figure 3.6: Image of a 1 ft. tilted square plate. Elevation 45°; VP; calculated data.

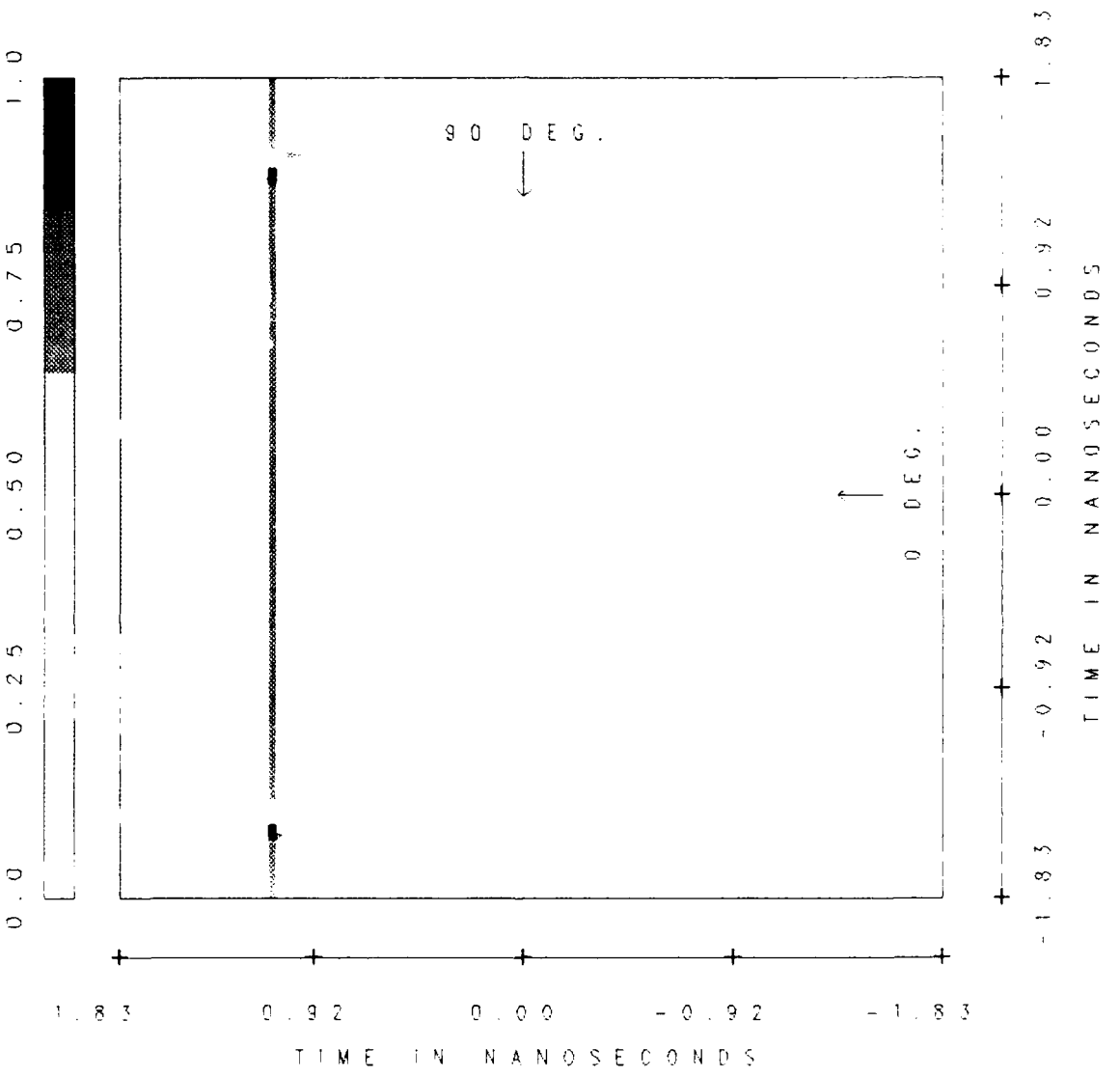

Figure 3.7: Image of a 1 ft. tilted square plate with a 90° spatial window. Elevation = 45°; VP; measured data.

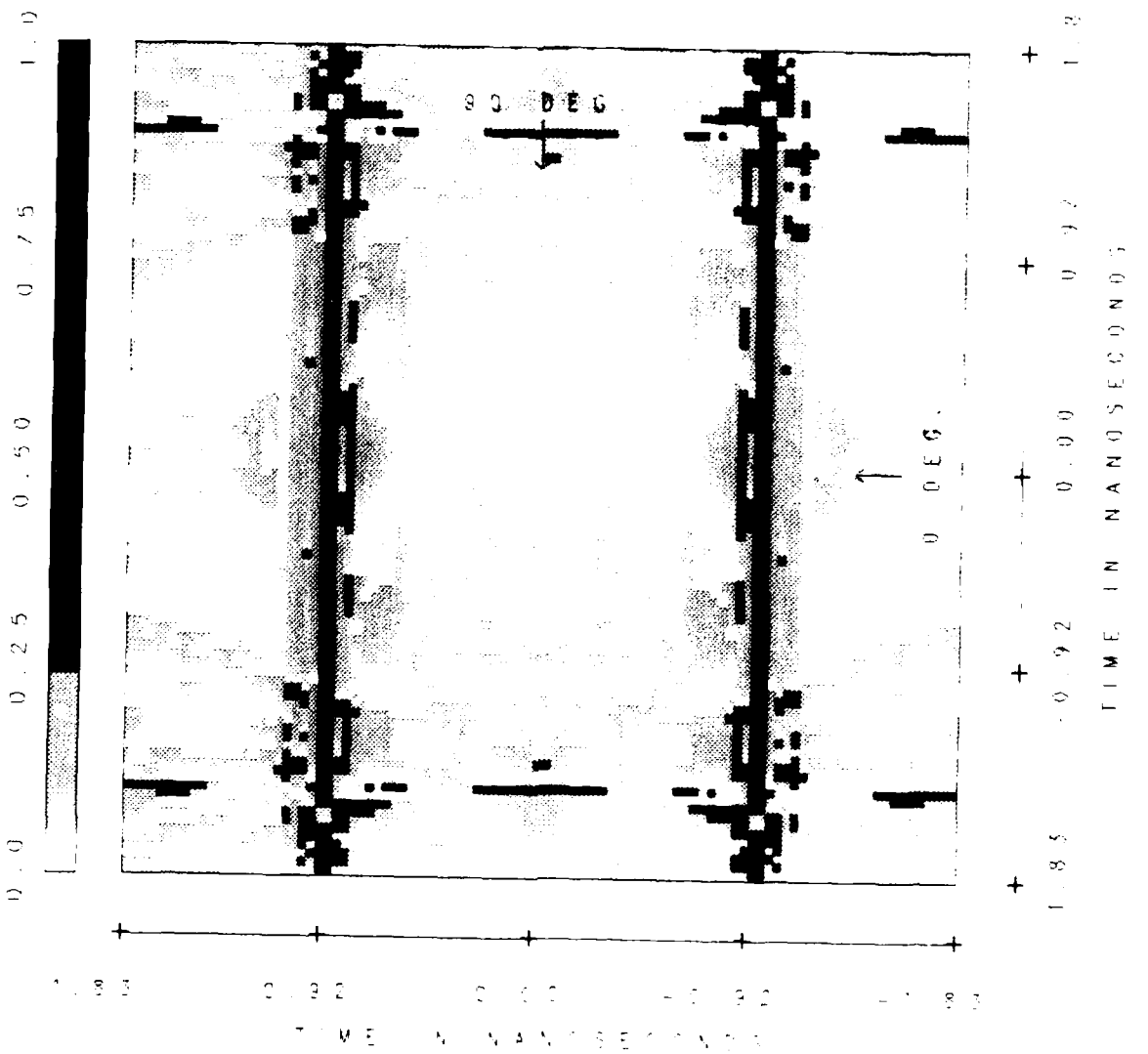

Figure 3.9: Image of a 1 ft. tilted square plate. Elevation 45°; HP; measured data.

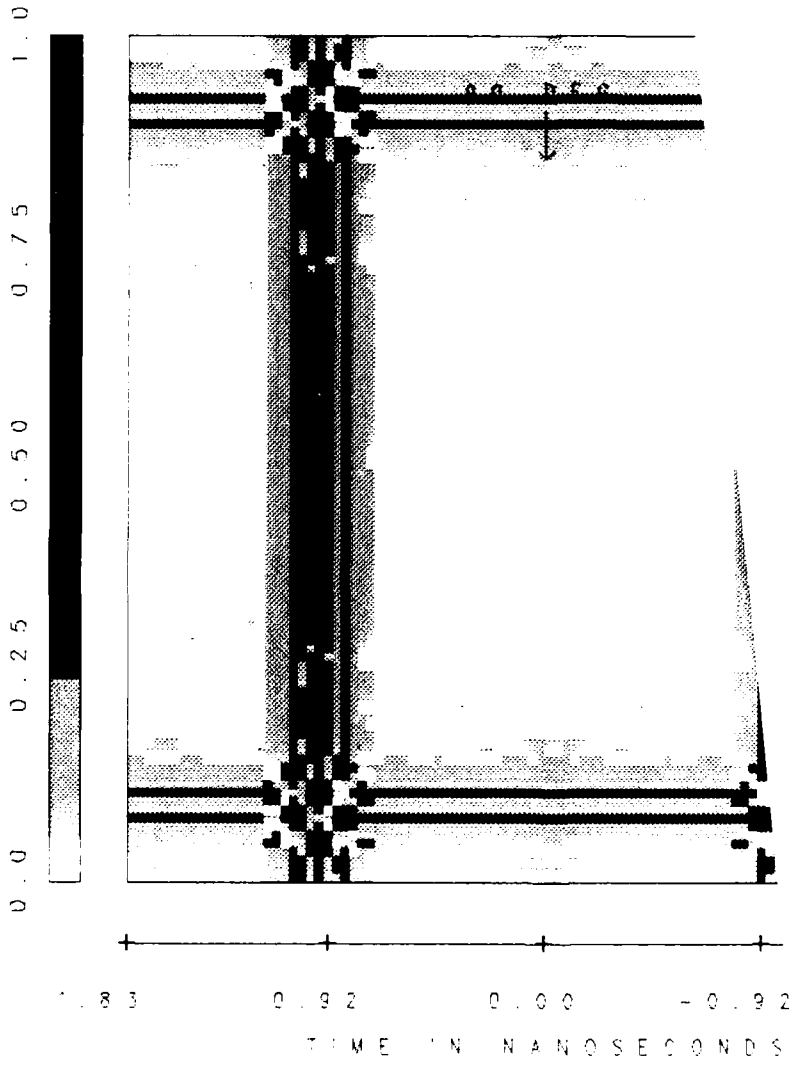

Figure 3.10: Image of a 1 ft. tilted square plate. Elevation data.

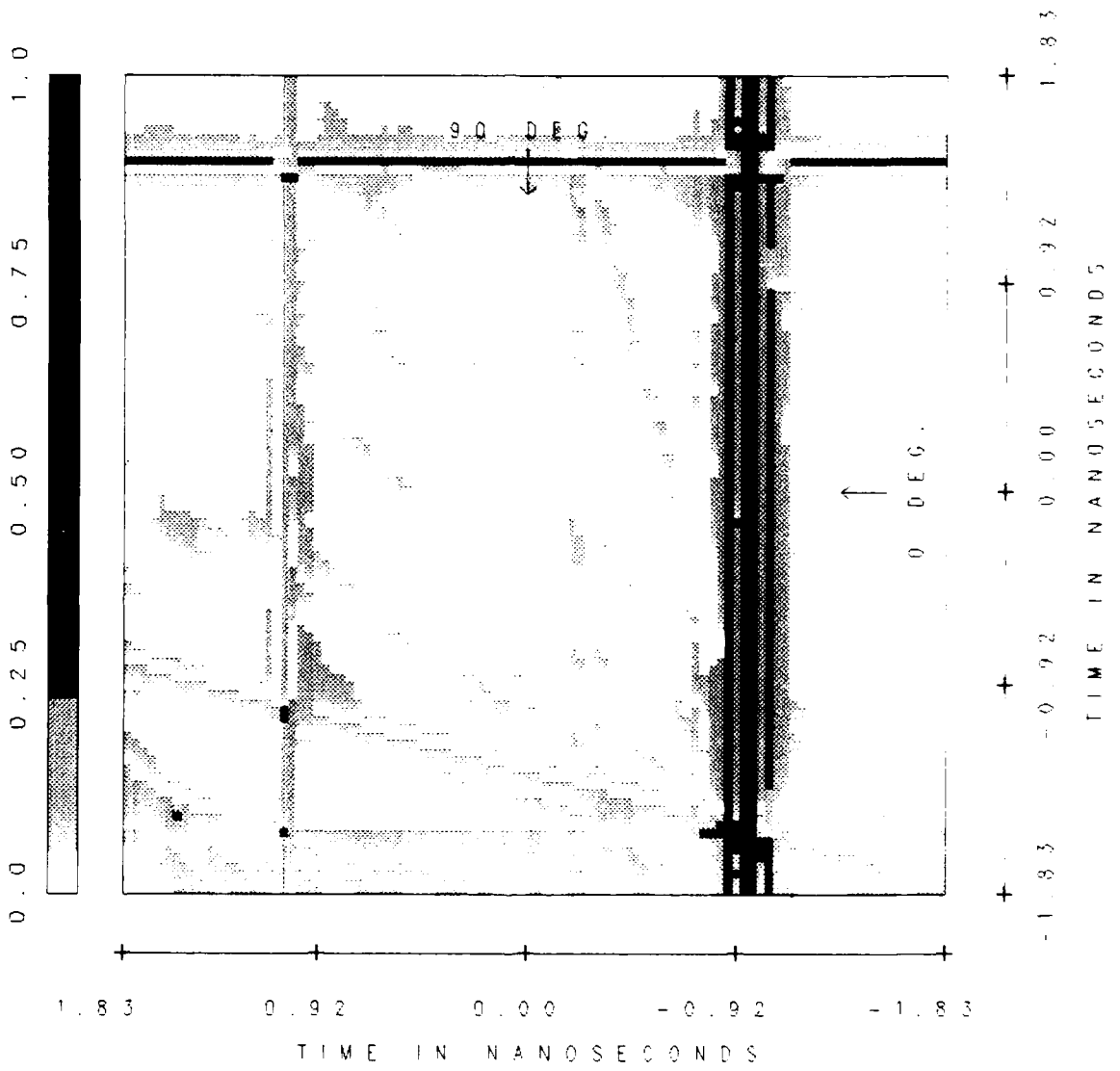

Figure 3.11: Image of a 1 ft. tilted square plate with a 90° spatial window. Elevation = 45°; HP; measured data.

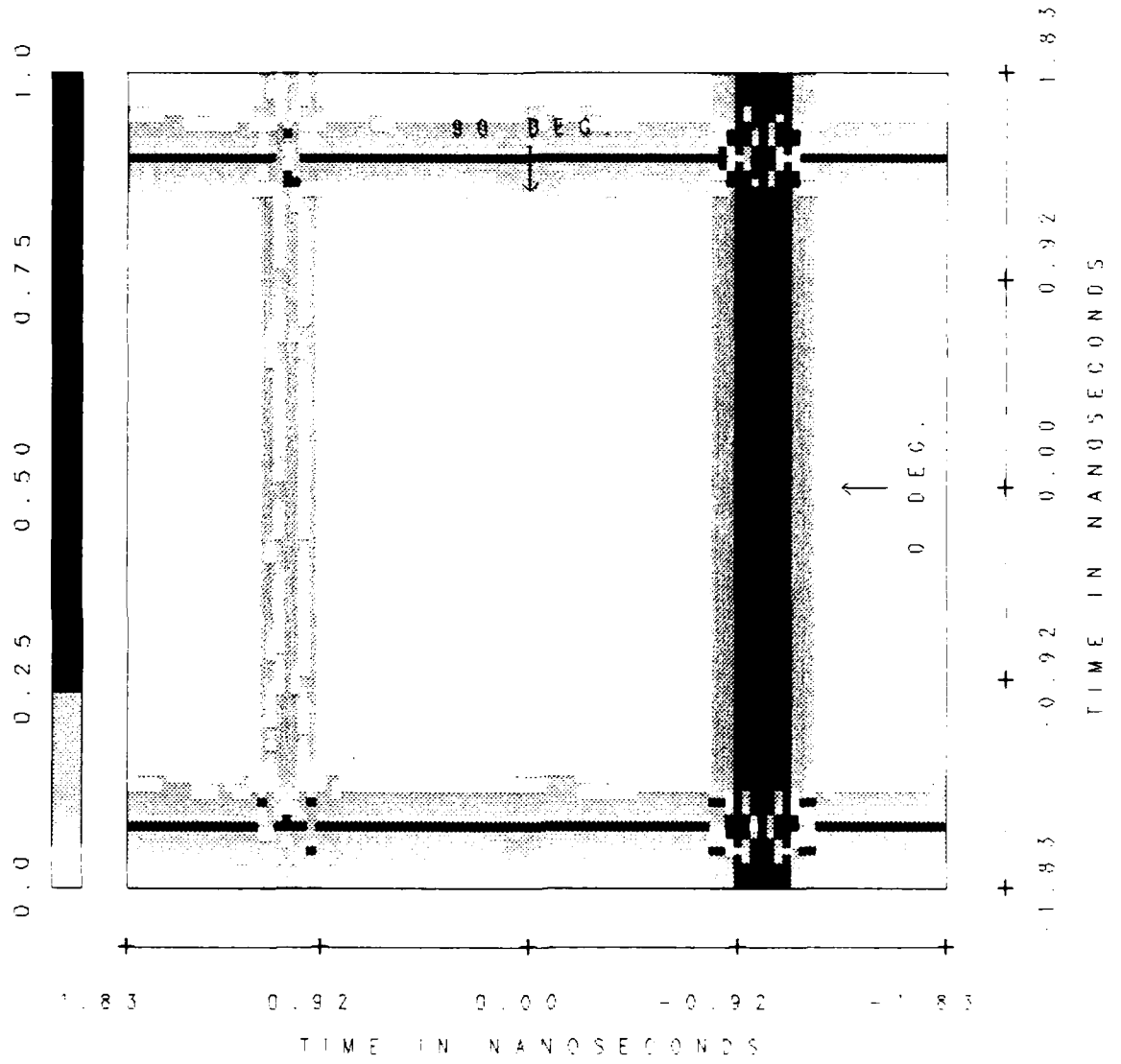

Figure 3.12: Image of a 1 ft. tilted square plate with a 90° spatial window. Elevation = 45°; HP; calculated data.

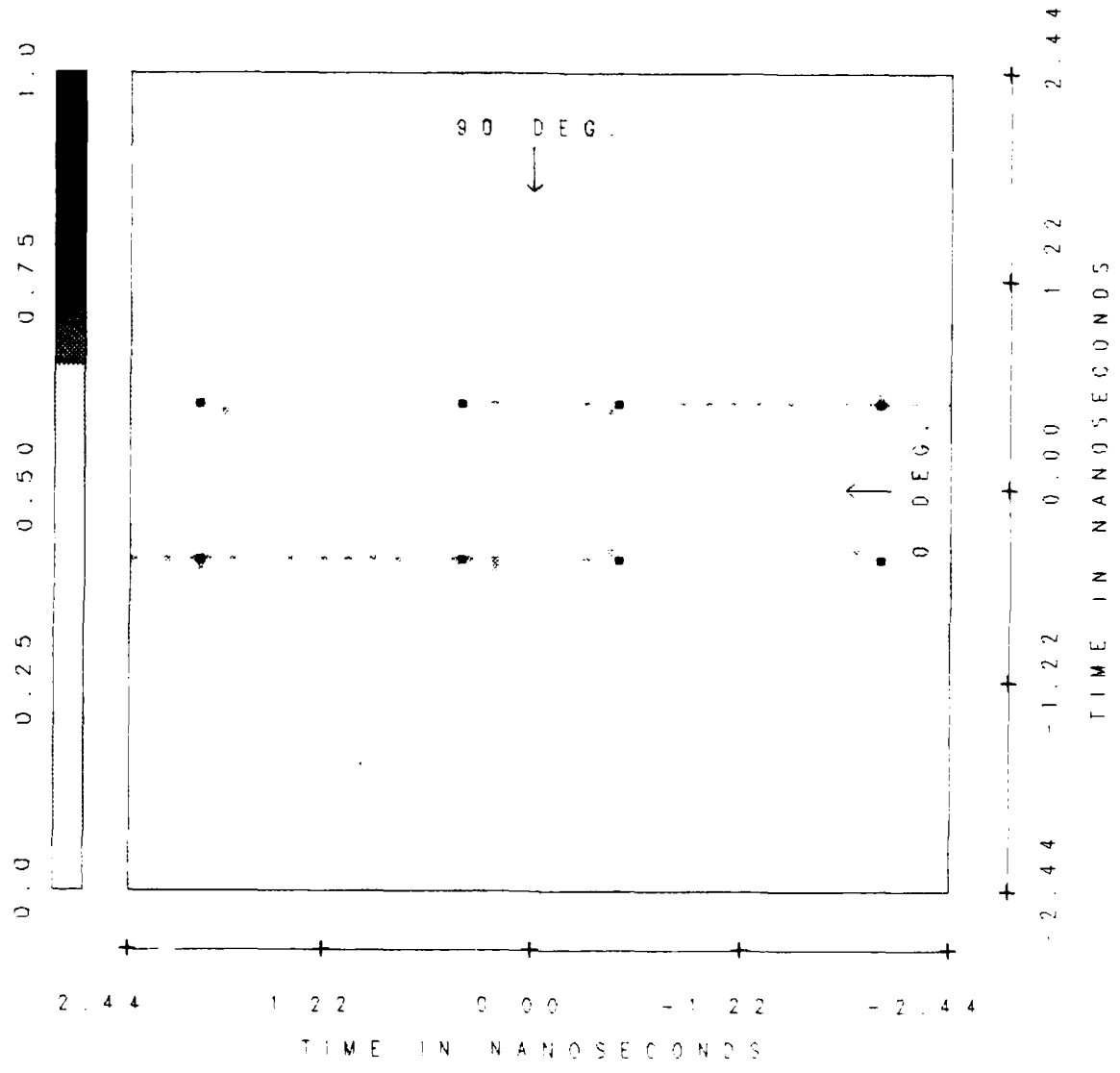

Figure 3.13: Image of an ellipsoid. Elevation = 0°; VP.

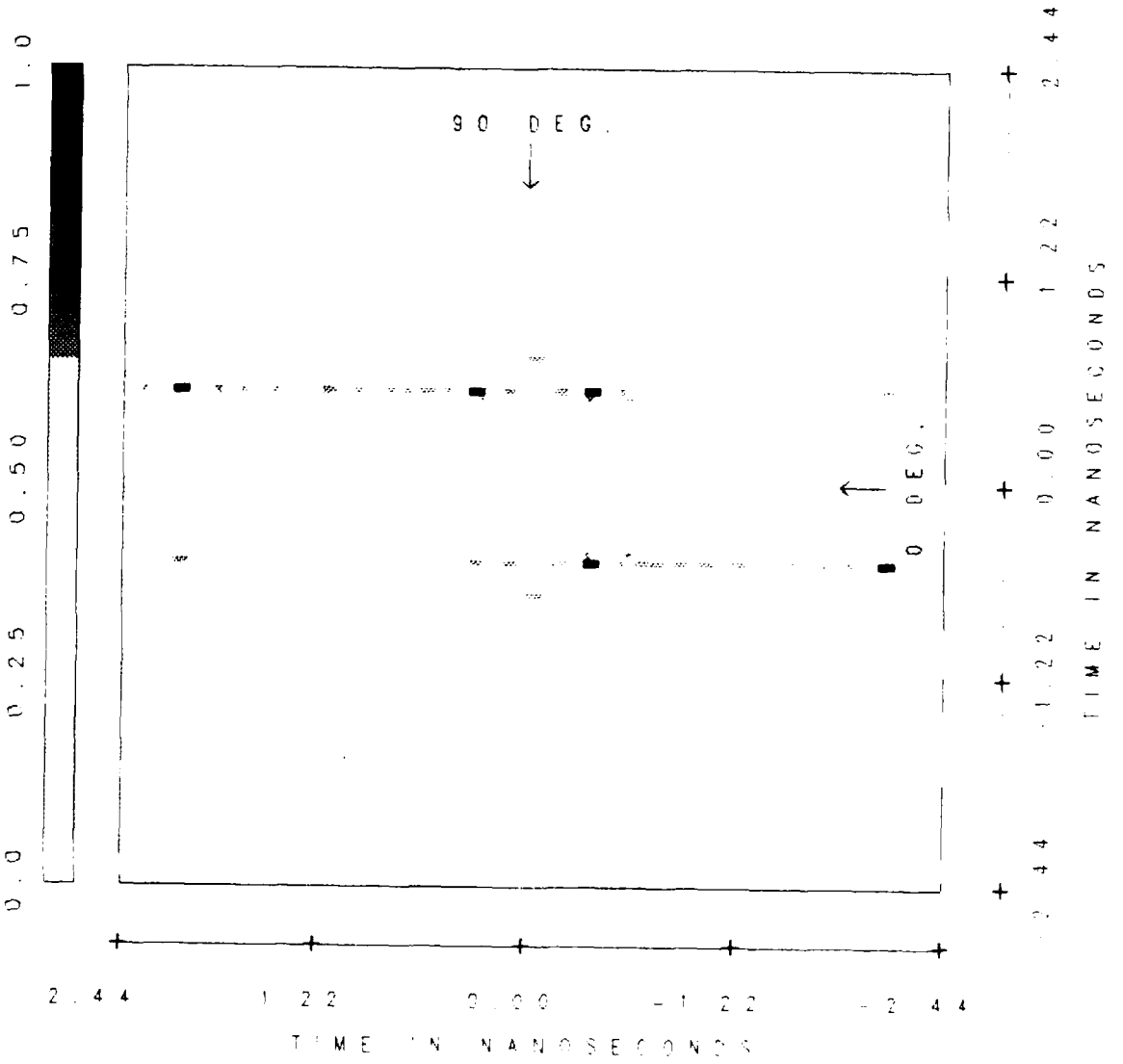

Figure 3.14: Image of a tilted ellipsoid. Elevation = 30°; VP.

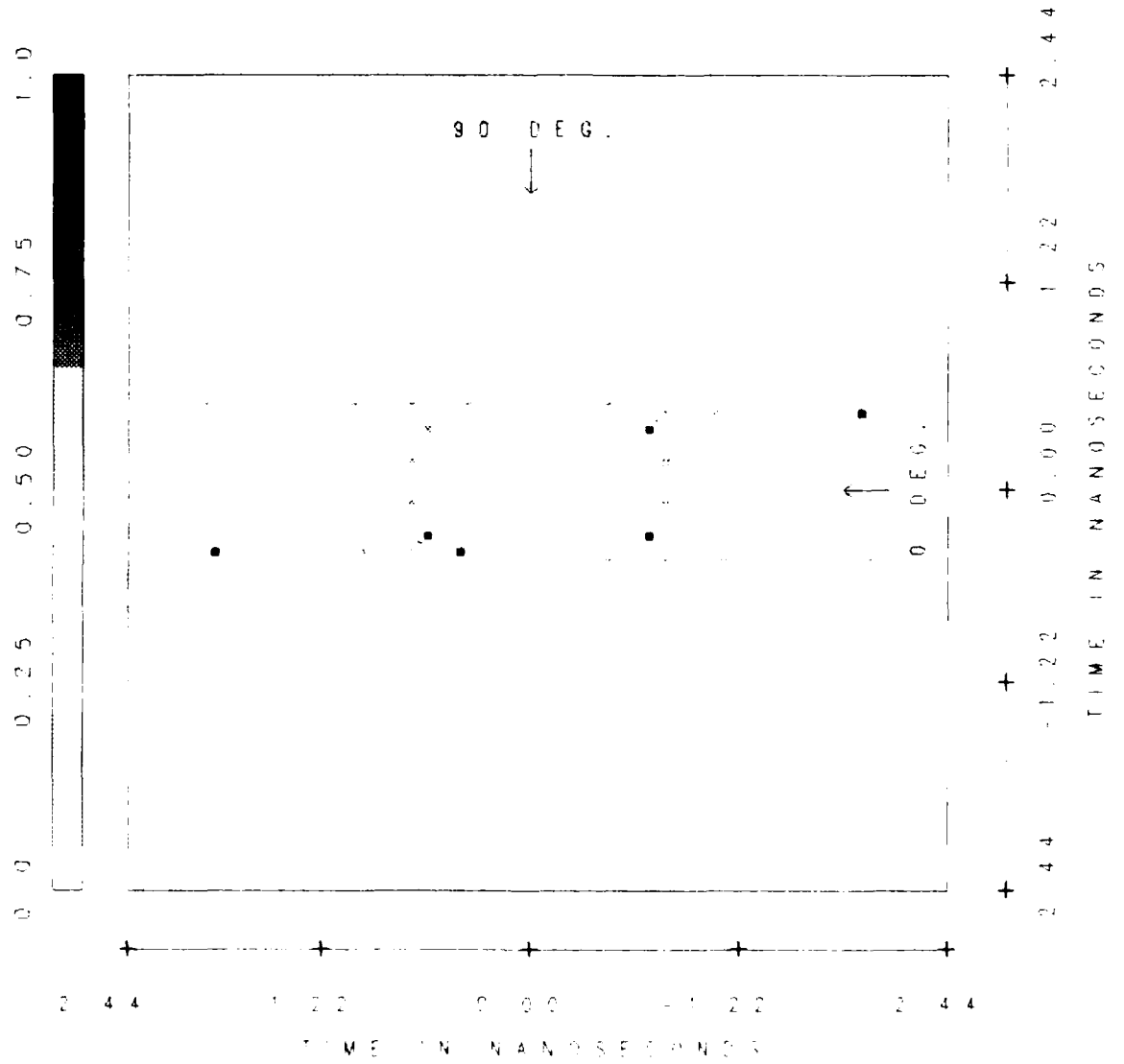

Figure 3.15: Image of a tilted ellipsoid. Elevation = 60°; VP.

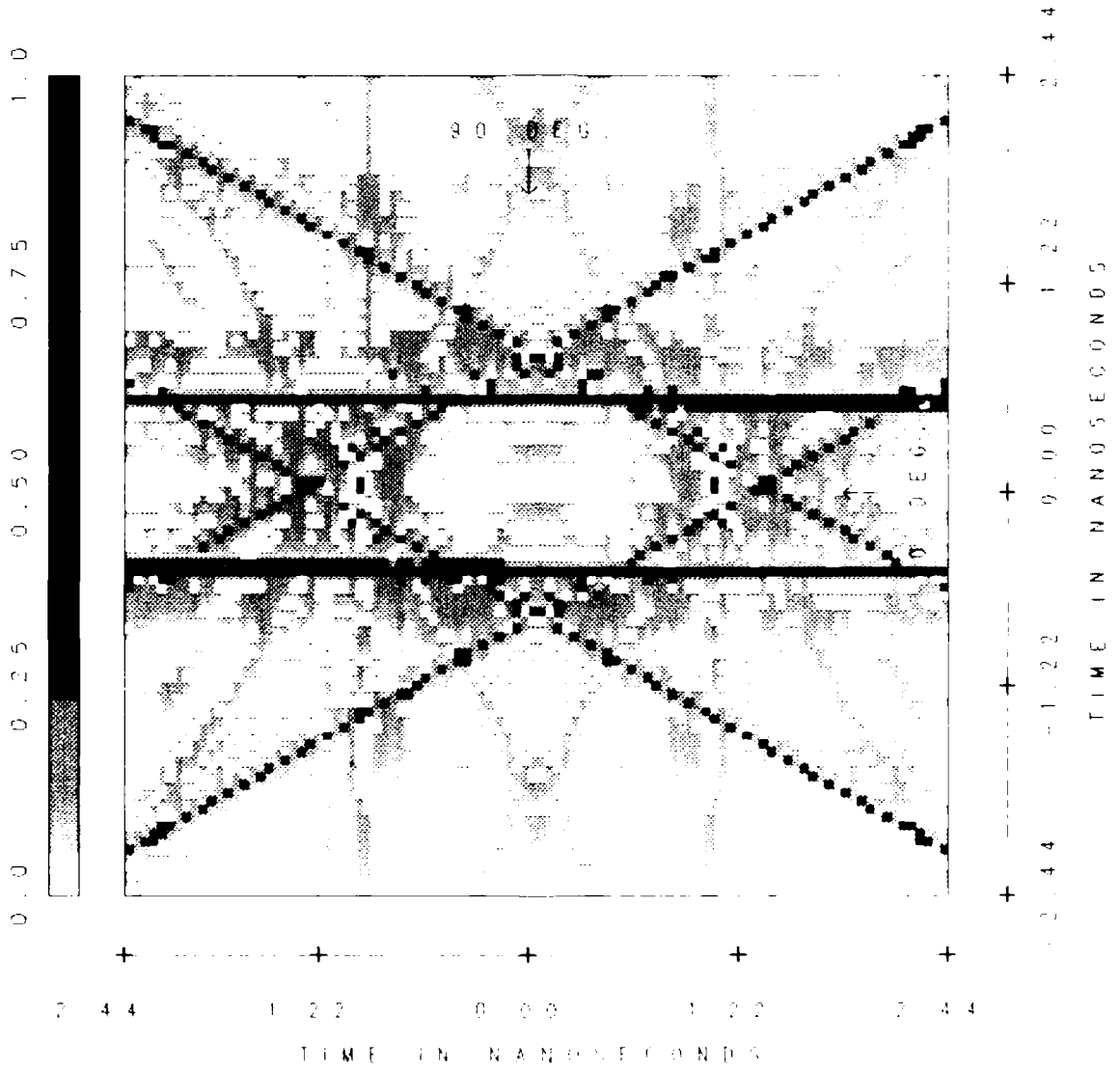

Figure 3.16: Image of an ellipsoid. Elevation = 0°; HP.

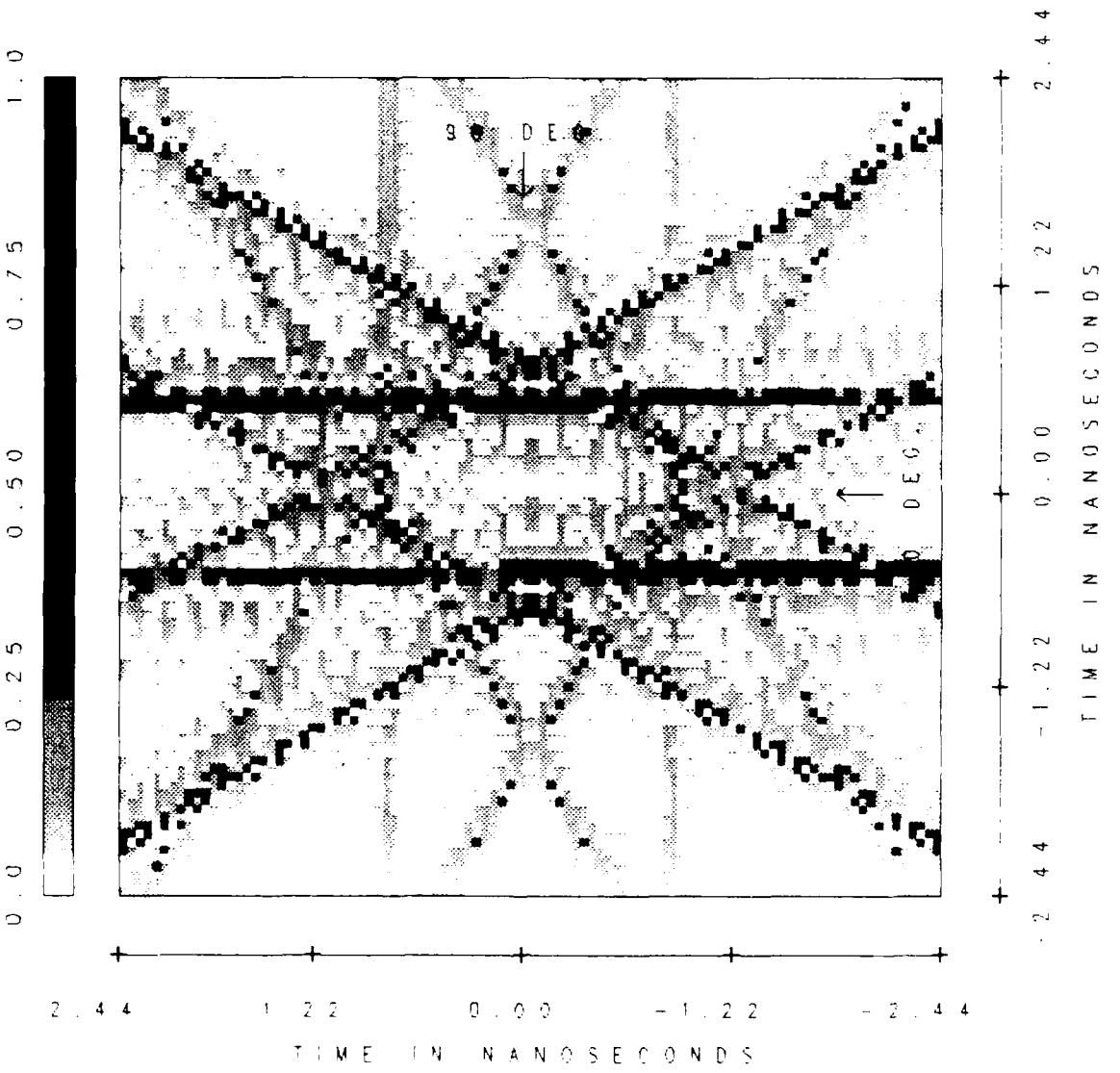

Figure 3.17: Image of a tilted ellipsoid. Elevation = 30°; HP.

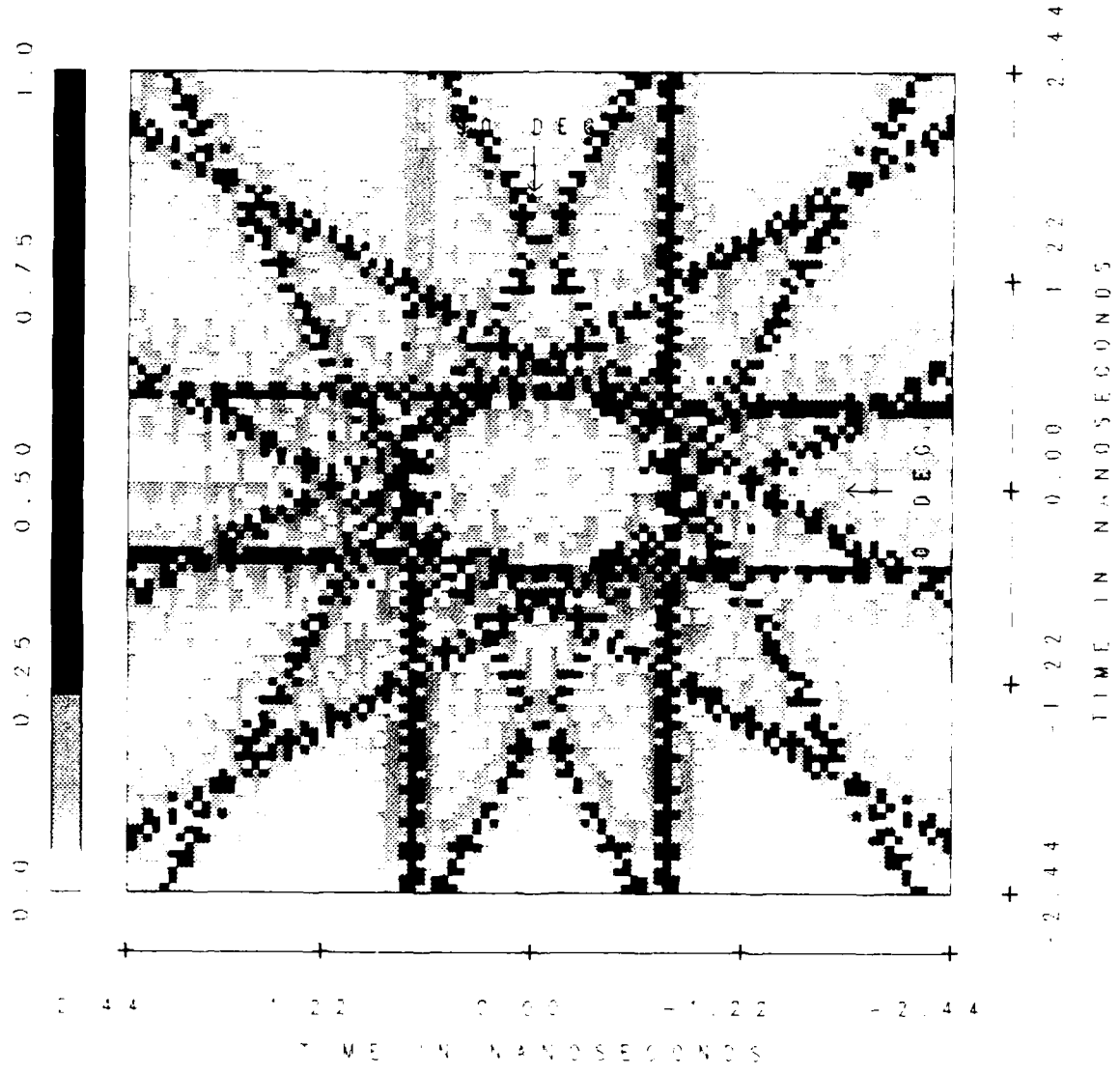

Figure 3.18: Image of a tilted ellipsoid. Elevation = 60°; HP.

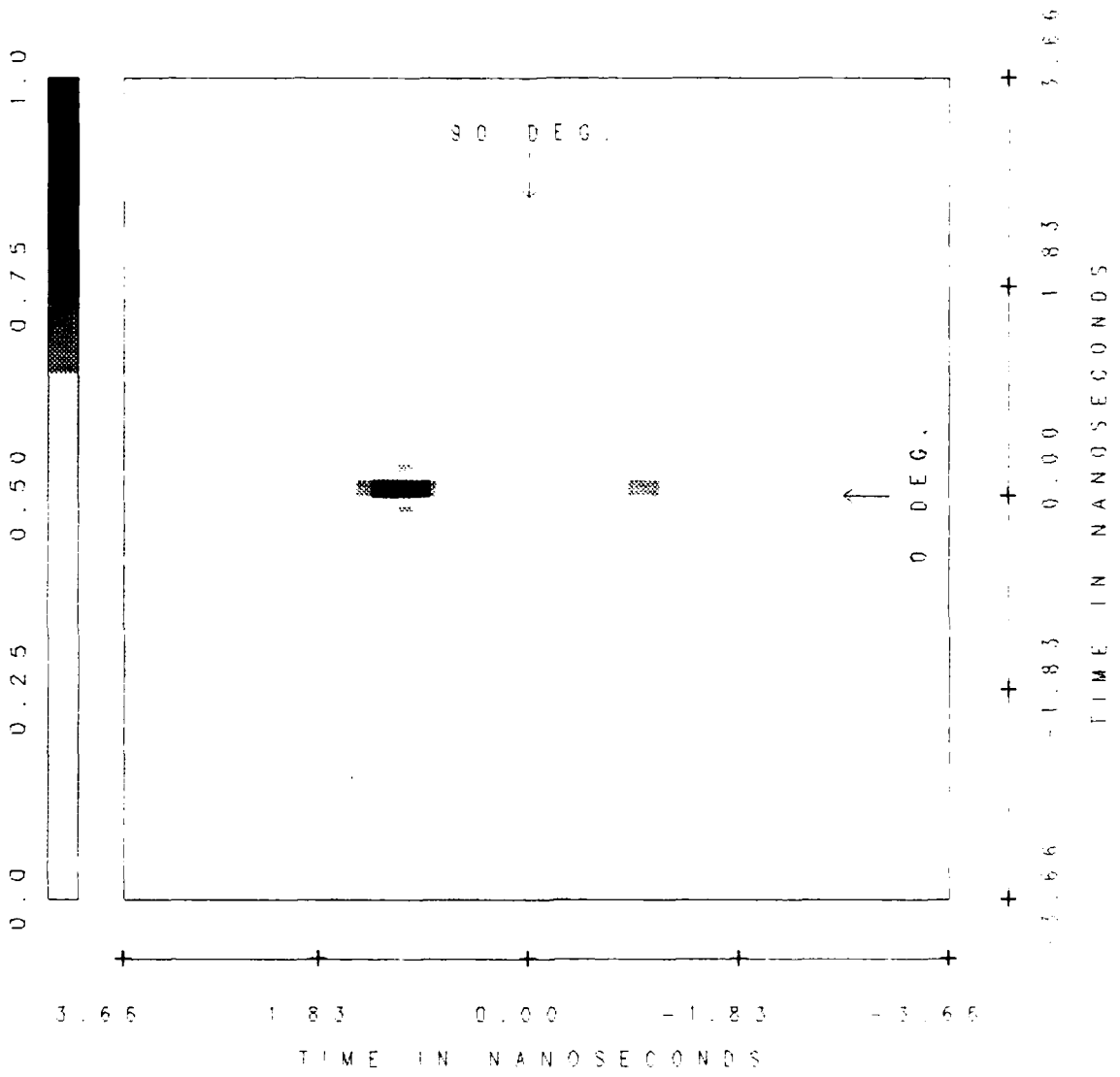

Figure 3.19: Image of a Boeing 707 aircraft; VP.

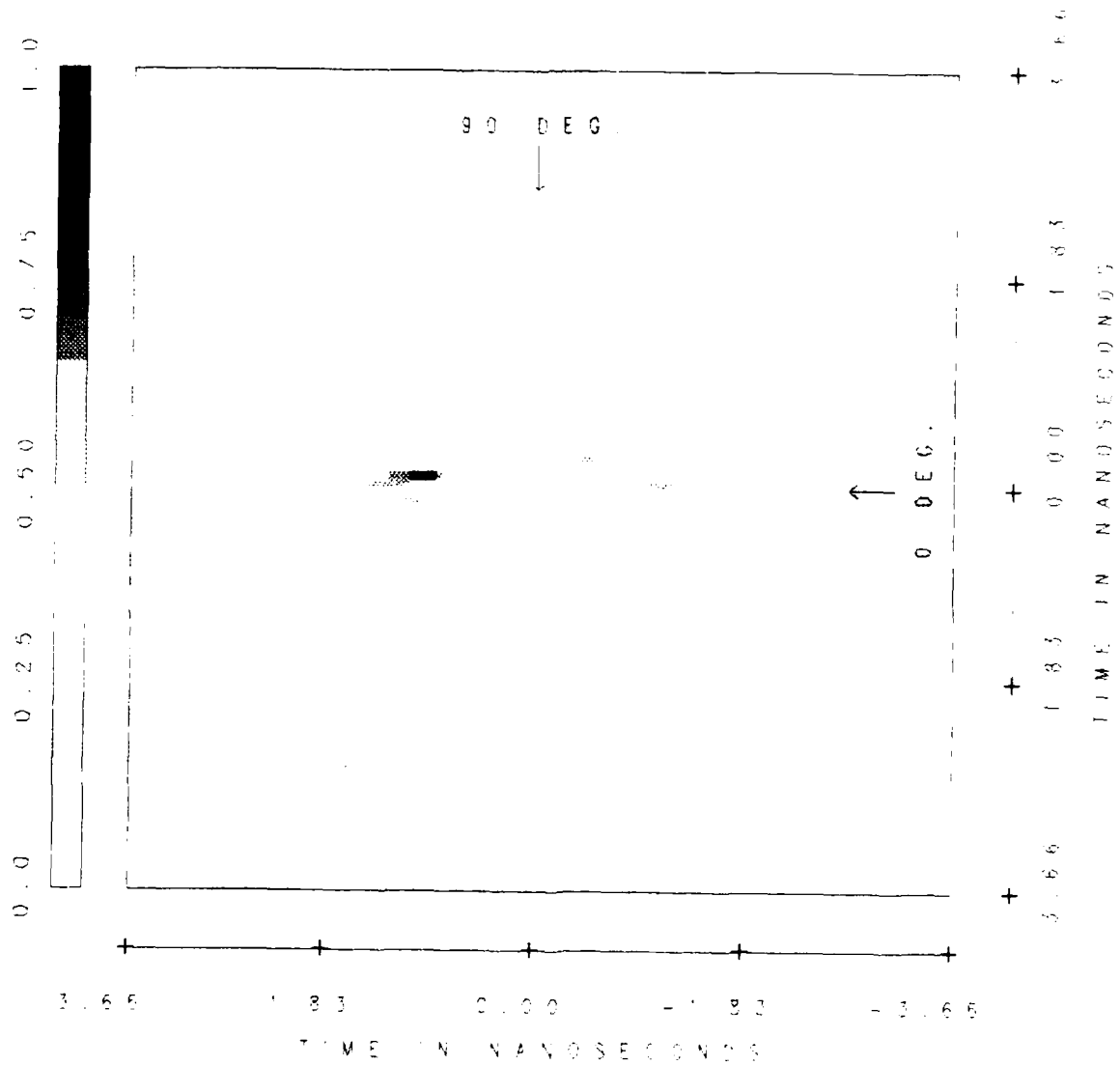

Figure 3.20: Image of a Boeing 707 aircraft with 180° spatial window, VP.

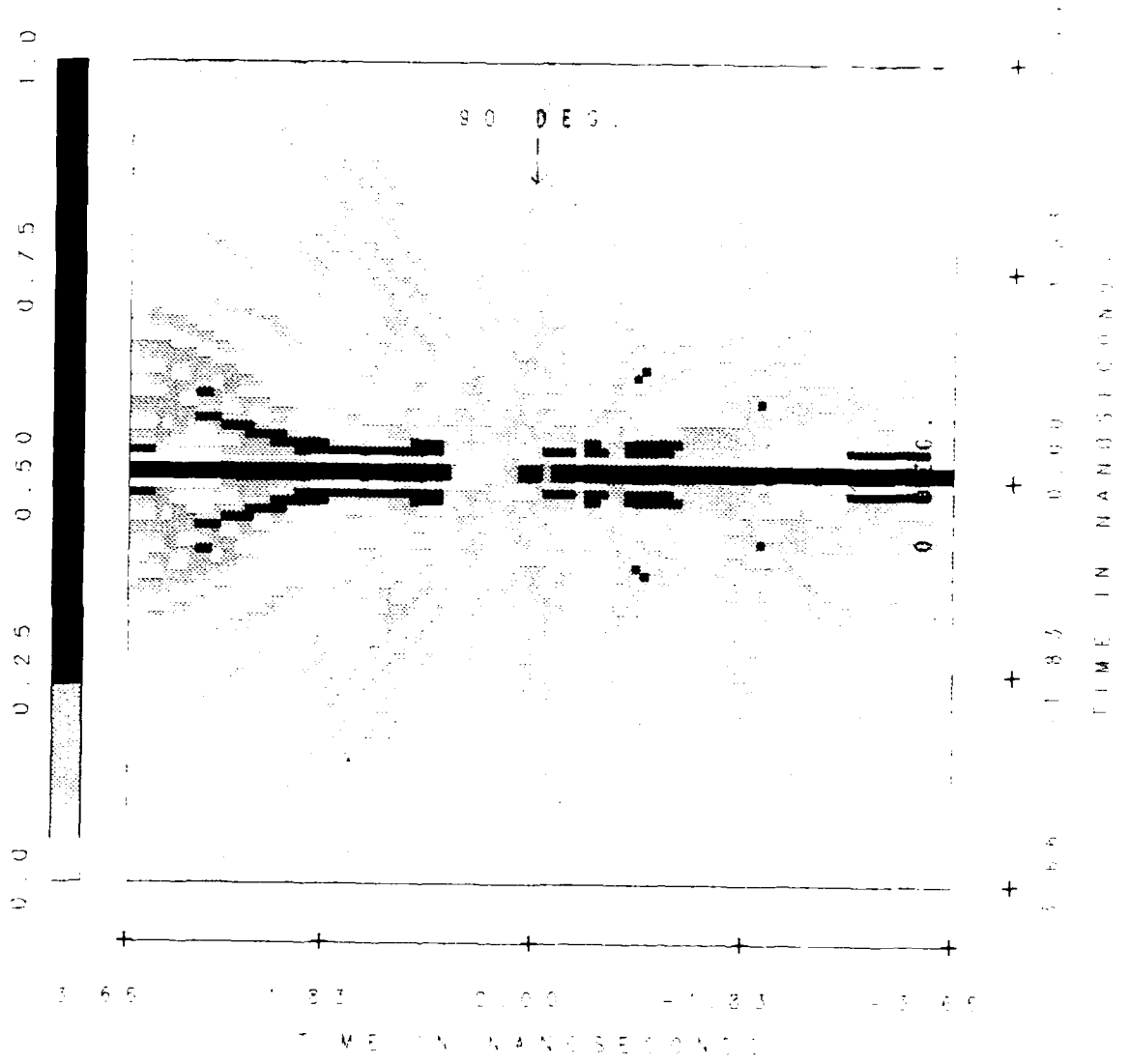

Figure 3.21: Image of a Boeing 707 aircraft, HP.

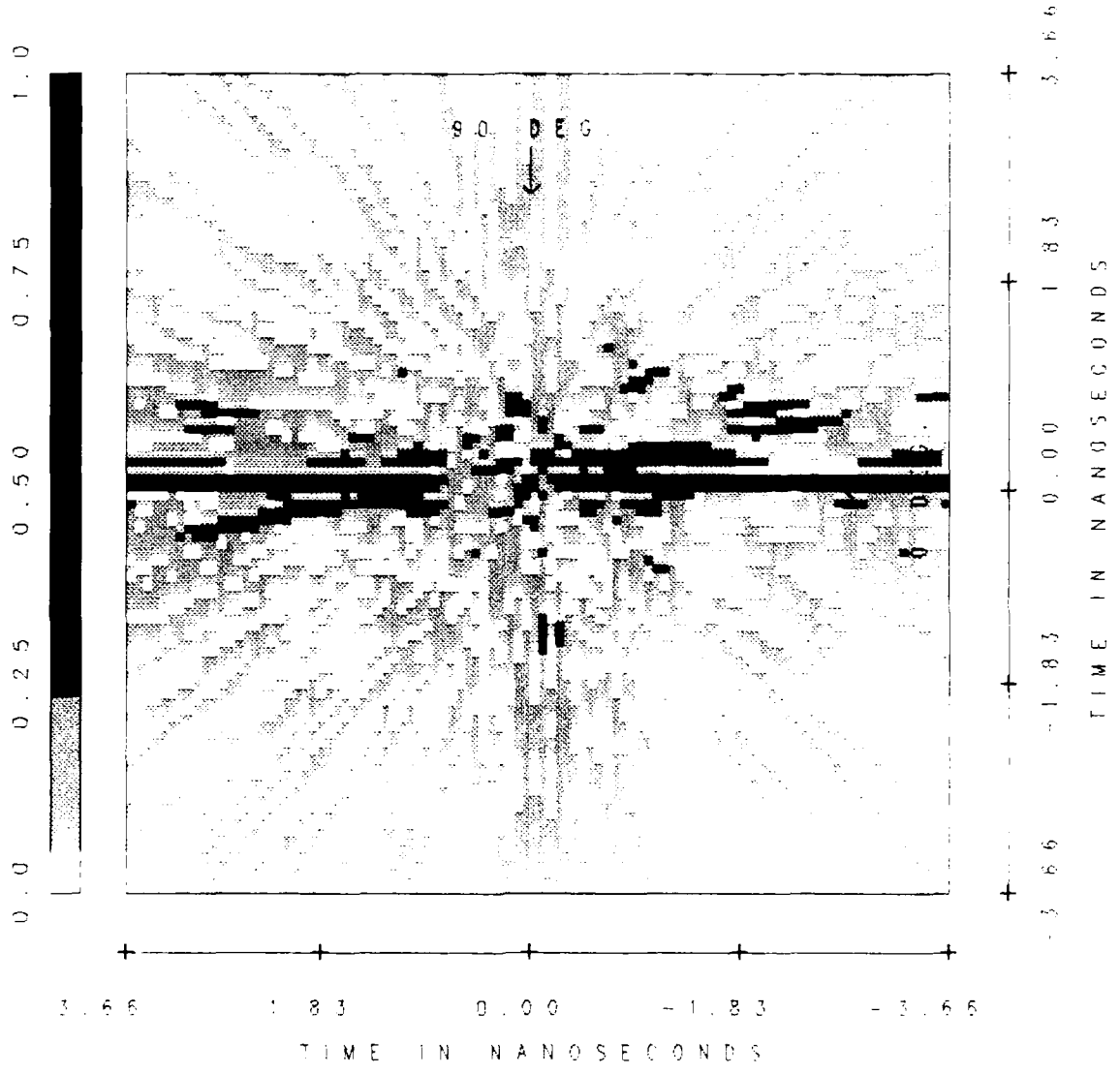

Figure 3.22: Image of a Boeing 707 aircraft with 180° spatial window, HP.

4. CONCLUSIONS

It was shown that the 2-D image of the target is related to its 2-D frequency spectra by a Fourier transform relationship. However, the frequency domain data is sampled on a polar raster and needs to be transformed into a rectangular one. The imaging algorithm described in this report substitutes for conventional 2-D Fourier transform and avoids the errors due to interpolation by using a 1-D inverse Fourier transform and a summation procedure. Hence, it improves the quality of the images.

Images are polarization dependent because the scattering properties of most scatterers are polarization dependent. Use of polarization information as a new dimension in images makes them more uniquely identifiable. Use of color helps different scattering centers related to different polarizations to be identified, especially when the images corresponding to different polarizations are combined in the same frame which may be a part of the future research as a continuation of the work described here.

A sphere, tilted square plate, tilted ellipsoid and a Boeing 707 aircraft are the targets investigated in this research. The geometrically simple ones help to understand the basic scattering characteristics. The square plate was studied both with measured and theoretical data. Results are found to be in good agreement, and polarization is found to be a useful tool for target recognition and identification with imaging. More work is required to be done to improve the aircraft images.

5. REFERENCES

[1] J.D. Young, "Target Imaging from Multiple-Frequency Radar Returns," Technical Report 2768-6, The Ohio State University ElectroScience Laboratory, Department of Electrical Engineering, Columbus, Ohio, generated under Grant No. AFOSR-69-1710, for Department of the Air Force, Air Force Office of Scientific Research, Arlington, Virginia, 1971.

[2] F. Jay, *IEEE Standard Dictionary of Electrical and Electronic Terms*, IEEE Inc., New York, New York, p. 361, 1977.

[3] R.M. Lewitt, "Reconstruction Algorithms: Transform Methods," *Proc. IEEE*, Vol. 71, No. 3, pp. 390-408, March 1983.

[4] D.L. Mensa, *High Resolution Radar Imaging*, Artech House, Inc., Dedham, Massachusetts, 1981.

[5] D.L. Mensa, S. Halevy and G. Wade, "Coherent Doppler Tomography for Microwave Imaging," *Proc. IEEE*, Vol. 71, No. 3, pp. 254-261, March 1983.

[6] E.K. Walton and J.D. Young, "The Ohio State University Compact Radar Cross-Section Measurement Range," *IEEE Trans. on Antennas and Propagation*, Vol. AP-32, No. 11, pp. 1218-1223, November 1984.

[7] R.J. Marhefka, "UTD Scattering from Structures Including Higher Order Terms," Technical Report 718295-3, The Ohio State University ElectroScience Laboratory, Department of Electrical Engineering, Columbus, Ohio, generated under Contract No. F33615-86-K-1023, for Department of the Air Force, AFWAL/AAWP-3, Wright-Patterson AFB, Ohio, 1986.

[8] D.E. Dudgeon and R.M. Merserau, *Multidimensional Digital Signal Processing*, Prentice-Hall, Englewood Cliffs, New Jersey, pp. 360-367, 1984.

[9] A.C. Kak, "Tomographic Imaging with Diffracting and Non-Diffracting Sources," in *Array Signal Processing Systems*, Simon Haykin, Ed., Prentice-Hall, Englewood Cliffs, New Jersey, 1984.

[10] A. Kak and M. Slaney, *Principles of Computerized Tomographic Imaging*, a draft book to be published by the IEEE press.

[11] A. Paploulis, *Fourier Integral and Its Applications*, McGraw-Hill, New York, New York, 1962.

[12] C.E. Shannon, "Communication in the Presence of Noise," IRE Proceedings, January 1949.

[13] F.Y.S. Fok, "Space Frequency Sampling Criteria for Electromagnetic Scattering of a Finite Object," Technical Report 714190-11, The Ohio State University ElectroScience Laboratory, Department of Electrical Engineering, Columbus, Ohio, generated under Contract No. N00014-83-K-0037, for Department of the Navy, Office of Naval Research, Arlington, Virginia, 1985.

[14] G. Sinclair, "The Transmission and Reception of Elliptically Polarized Waves," *Proc. IRE*, pp. 148-151, February 1950.

[15] E.M. Kennaugh, "Polarization Properties of Radar Reflections," OSU Antenna Laboratory Report 389-12, generated under Contract No. AF 28(099)-90, for Rome Air Development Center, Griffiss AFB, New York, March 1952.

[16] C.D. Graves, "Radar Polarization Power Scattering Matrix," *Proc. IRE*, pp. 248-252, February 1956.

[17] W.M. Boerner, B.E. Mohamed, C.Y. Chan and P.M. Mastoris, "Polarization Dependence in Electromagnetic Inverse Problems," *IEEE Trans. on Antennas*

and Propagation, Prentice-Hall, Englewood Cliffs, New Jersey, pp. 360-367, 1984.

[18] A.B. Kostinski and W.M. Boerner, "On Foundations of Radar Polarimetry," *IEEE Trans. on Antennas and Propagation*, Vol. AP-34, No. 2, pp. 1394-1404, December 1986.

[19] J.W. Leeper, "Identification of Scattering Mechanisms from Measured Impulse Response Signatures of Several Conducting Objects," *M.Sc. thesis*, The Ohio State University, Columbus, Ohio, 1983.

[20] F.A. Sitka, "UTD Analysis of Electromagnetic Scattering by Flat Plate Structures," Technical Report 711930-2, The Ohio State University ElectroScience Laboratory, Department of Electrical Engineering, Columbus, Ohio, generated under Grant No. NSG 1613, for National Aeronautics and Space Administration – Langley Research Center, Hampton, Virginia, December 1981.

[21] E.M. Kennaugh and D.L. Moffatt, "Transient and Impulse Response Approximations," *Proc. IEEE*, Vol. 53, No. 8, pp. 893-901, August 1965.

[22] G. Dural, S. Smithberger and J.D. Young, "CIMAG2: The Computer Program to Generate Color Images," Technical Report 718048-7, The Ohio State University ElectroScience Laboratory, generated under Contract No. N00014-86-K-0202, for Department of the Navy, Office of Naval Research, Arlington, Virginia, in preparation.

6. APPENDIX

THE COMPUTER PROGRAM CLRPL

THE SOFTWARE CODE TO DISPLAY IMAGES ON THE TEKTRONIX 429 COLOR CRT DISPLAY.

```
CCCCCCCCCCCCCCCCCCCCCCCCCCCCCCCCCCCCCCCCCCCCCCCCCCCCCCCCCCCCCCCCCCCCCCC
CCCCCCCCCCCCCCCCCCCCCCCCCCCCCCCCCCCCCCCCCCCCCCCCCCCCCCCCCCCCCCCCCCCCCCC
CC                                                                    CC
CC                              CLRPL                                 CC
CC                                                                    CC
CCCCCCCCCCCCCCCCCCCCCCCCCCCCCCCCCCCCCCCCCCCCCCCCCCCCCCCCCCCCCCCCCCCCCCC
CCCCCCCCCCCCCCCCCCCCCCCCCCCCCCCCCCCCCCCCCCCCCCCCCCCCCCCCCCCCCCCCCCCCCCC
C
C
C
C       THIS PROGRAM DEFINES A PLOTTING SOFTWARE CODE TO PLOT
C       IMAGE OF AN OBJECT WITH POLARIZATION INFORMATION
C
C       IMAGE DATA SHOULD BE CODED BY A 100*100 MATRIX AND
C       IT SHOULD BE CONTAINED IN THE MATRIX 'ARRAY(100,100)'

        DIMENSION ICOL(100,100),ICOLA(100)
        DIMENSION GX(5),GY(5),CBX(5),CBY(5),XP(5),YP(5),XT(10),YT(10)
        DIMENSION ARRAY(100,100),COORD(5)
        INTEGER COLI,WKSTID
        REAL*4 L
        LOGICAL FINISHED
        CHARACTER*40 FILNM
        CHARACTER*7 NUMB

C       THE GX MATRIX IS THE X COORDINATES OF THE COLOR GRID
        DATA GX/.30,.85,.85,.30,.30/

C       THE GY MATRIX IS THE Y COORDINATES OF THE COLOR GRID
        DATA GY/.12,.12,.67,.67,.12/

C       THE CBX MATRIX IS THE X COORDINATES OF THE COLOR BOX
        DATA CBX/.30,.85,.85,.30,.30/

C       THE CBY MATRIX IS THE Y COORDINATES OF THE COLOR BOX
        DATA CBY/.70,.70,.72,.72,.70/

C       THE XT MATRIX IS THE X COORDINATES OF THE TIK MARKS
        DATA XT/.3,.44,.57,.71,.85,.26,.26,.26,.26,.26/

C       THE YT MATRIX IS THE Y COORDINATES OF THE TIK MARKS ON THE Y AXIS
        DATA YT/.08,.08,.08,.08,.08,.12,.26,.40,.54,.67/


        PI=4.*ATAN(1.)
        KWK=412505
        WKSTID=1

C
C       YMTCL--Y Value of Magnitude Top Center Line
        YMTCL=CBY(3)+.02
C
C       ENTER THE ARRAY TO BE PLOTTED
        WRITE(6,*)'ENTER FILE NAME'
        READ(5,100) FILNM
100     FORMAT(A40)
C
C
C       POLARIZATION DEPENDENT PLOT?
        WRITE(6,*) 'DO YOU NEED TO USE POLARIZATION AS A PARAMETER?'
        WRITE(6,*)'(Y=1 N=0)'
        READ(5,*) POL
        IF(POL.EQ.1) THEN
C       ENTER THE POLARIZATION
        WRITE(6,*)'ENTER POLARIZATION (VP=1,HP=2)'
        READ(5,*) PL
```

```
        ELSE
        END IF
C
        OPEN(UNIT=1,FILE=FILNM,STATUS='OLD',FORM='UNFORMATTED')
C
C       ENTER THE IMAGE SIZE AND PERIOD OF THE TIME SIGNAL
        READ(1) IMGSZ,PER
C
C       ENTER THE IMAGE ARRAY

        DO 1000 I=1,100
        DO 1000 J=1,100
        READ(1)ARRAY(I,J)
        ARRAY(I,J)=ABS(ARRAY(I,J))
1000    CONTINUE
C


C       NORMALIZE THE ARRAY VALUES
C
        CALL SEARCH(ARRAY,AMAX,AMIN)
        WRITE(6,*)'MAX=',AMAX,'MIN=',AMIN
        WRITE(6,*)'ENTER THE DESIRED MAX.,AND,MIN.'
        READ(5,*) ANMAX,ANMIN
        DO 20 I=1,100
        DO 20 J=1,100
        IF (ARRAY(I,J).GT.ANMAX) ARRAY(I,J)=ANMAX
        IF (ARRAY(I,J).LT.ANMIN) ARRAY(I,J)=ANMIN
        ARRAY(I,J)=(ARRAY(I,J)-ANMIN)/(ANMAX-ANMIN)
20      CONTINUE
C
C       OPEN GKS ERROR FILE
        CALL GOPKS(6,5000)

C       FIND CONNECT ID
999     CALL GKHGCI('ESL 4129',JERROR,KCONID)
        IF(JERROR.NE.0) THEN
        WRITE(6,*) 'Can not be a connection ID'
        WRITE(6,*) 'Would you like to wait ? (Y=1)'
        READ(5,*)ANS
        IF(ANS.NE.1) THEN
           STOP
           ELSE
            WRITE(6,*) 'Enter 1 when ready'
            READ(5,*) ANS
            GO TO 999
        END IF
        END IF
C       OPEN WORKSTATON #1
        CALL GOPWK(1,KCONID,KWK)

C       ACTIVATE WORKSTATION #1
        CALL GACWK(1)

C       SET THE WORKSTATION WINDOW/VIEWPORT-FULLSCREEN
C       GET MAX X AND Y
        KUNITS=0
        CALL GQDSP(KWK,KERROR,KUNITS,XSIZE,YSIZE,KRASX,KRASY)
        CALL GSWKWN(1,0.,1.,0.,YSIZE/XSIZE)
        CALL GSWKVP(1,0.,.343,0.,.274)

C       GENERATE THE COLOR INDICES
C
       IF(POL.EQ.0) THEN
         DO 3 COLI=1,100
                L=.5
                S=1
```

```
                IF(COLI.LE.5)L=0
                H=95+2.6*COLI
                CALL HLSRGB(H,L,S,R,G,B)
                CALL GSCR(1,1+COLI,R,G,B)
                ICOLA(COLI)=1+COLI
3       CONTINUE
                ELSE
               DO 4 COLI=1,100
                L=.5
                S=1
                FC=25*(4.8)**(COLI/100.)
                IF(COLI.LE.5) L=0
                IF(PL.EQ.1) H=225-FC
                IF(PL.EQ.2)H=110-FC
                IF(PL.EQ.2.AND.COLI.LT.25.AND.COLI.GT.5)L=.75
                IF(H.LT.0) H=H+360
                CALL HLSRGB(H,L,S,R,G,B)
                CALL GSCR(1,1+COLI,R,G,B)
                ICOLA(COLI)=1+COLI
4       CONTINUE
        END IF
C
C       GENERATE COLOR CODE FOR X AND Y COORDINATED RCS LEVELS
        DO 30 I=1,100
           DO 30 J=1,100
             ICOL(I,J)=ARRAY(I,J)*99+2
30      CONTINUE

C       PLOT COLOR LABEL USING CELL ARRAY
        CALL GCRSG(SEG)
        CALL GCA(CBX(1),CBY(1),CBX(3),CBY(3),100,1,1,1,100,1,ICOLA)
        CALL GSPLCI(1)
        CALL GPL(5,CBX,CBY)
C

C       LABEL COLOR BAR
        CALL GSTXAL(2,3)
        CALL GSTXP(0)
        CALL GSCHXP(1.25)
        CALL GSCHSP(1.)
            CALL GTX(GX(1),YMTCL,'0.0')
            CALL GTX(.44,YMTCL,'0.25')
            CALL GTX(.57,YMTCL,'0.50')
            CALL GTX(.71,YMTCL,'0.75')
            CALL GTX(GX(2),YMTCL,'1.0')
            CALL GSCHXP(1.)
            CALL GSCHSP(1.)

C       PLOT COLOR MATIX USING CELL ARRAY
        TEST=10
        IF (TEST.EQ.0)GO TO 21
        CALL GCA(GX(1),GY(1),GX(3),GY(3),100,100,1,1,100,100,ICOL)
        CALL GSPLCI(1)
        CALL GPL(5,GX,GY)
C
C       DRAW GRID LINE ADJACENT TO EACH AXES

        XP(1)=.30
        XP(2)=.85
        YP(1)=.08
        YP(2)=.08
        CALL GPL(2,XP,YP)
        XP(1)=.26
        XP(2)=.26
        YP(1)=.12
        YP(2)=.67
```

```
      CALL GPL(2,XP,YP)

C     PRINT THE TIK MARKS

      CALL GSMK(2)
      CALL GSMKSC(1)
      CALL GSPMCI(1)
      CALL GPM(10,XT,YT)
C
C     SHOW THE ASPECT ANGLES
      XP(1)=.57
      XP(2)=.57
      YP(1)=.16
      YP(2)=.19
      CALL GPL(2,XP,YP)
      XP(1)=.565
      XP(2)=.57
      XP(3)=.575
      YP(1)=.185
      YP(2)=.19
      YP(3)=.185
      CALL GPL(3,XP,YP)
      XP(1)=.80
      XP(2)=.77
      YP(1)=.40
      YP(2)=.40
      CALL GPL(2,XP,YP)
      XP(1)=.775
      XP(2)=.77
      XP(3)=.775
      YP(1)=.405
      YP(2)=.4
      YP(3)=.395
      CALL GPL(3,XP,YP)
      CALL GTX(.57,.14,'0 DEG.')
      CALL GTX(.57,.02,'TIME IN NANOSECONDS')
      CALL GSTXAL(2,1)
      CALL GSTXP(0)
      CALL GSCHUP(1.,0.)
      CALL GTX(.82,.4,'90 DEG.')
      CALL GTX(.20,.40,'TIME IN NANOSECONDS')
C
C     FIGURE OUT THE COORDINATES ON EACH AXES
      CALL MARKS(IMGSZ,PER,COORD)
C
C     PRINT THE COORDINATES
      X=.30
      CALL GSCHUP(0.,1.)
      DO 40 I=1,5
      WRITE(NUMB,FMT='(F6.2)')COORD(I)
      CALL GTX(X,.06,NUMB)
40    X=X+.14
      CALL GSCHUP(1.,0.)
      Y=.12
      DO 50 I=1,5
      WRITE(NUMB,FMT='(F5.2)')COORD(I)
      CALL GTX(.23,Y,NUMB)
50    Y=Y+.14
C
C
C     COLOR 1 = WHITE, 0 = BLACK (ON PLOTTER, REVERSED ON SCREEN)
C
21    CALL GCLSG(SEG)
C
      WRITE(6,*)'Enter return to finish.....'
      READ(5,1)FINISHED
```

```
1       FORMAT(A1)
        CALL GCLRWK(WKSTID,1)            !Clears the screen on TEXTRONIX

C       DEACTIVATE THE WORK STATION
        CALL GDAWK(1)
C
C       CLOSE THE WORK STATION
        CALL GCLWK(1)

C       CLOSE THE SYSTEM
        CALL GCLKS
        STOP
        END


CCCCCCCCCCCCCCCCCCCCCCCCCCCCCCCCCCCCCCCCCCCCCCCCCCCCCCCCCCCCCCCCCCCCCCCCCCC
CC      THIS ROUTINE MAKES THE TRANSFORMATION BETWEEN COLOR SYSTEMS
CCCCCCCCCCCCCCCCCCCCCCCCCCCCCCCCCCCCCCCCCCCCCCCCCCCCCCCCCCCCCCCCCCCCCCCCCCC
C
        SUBROUTINE HLSRGB(H,L,S,R,G,B)
        REAL H,L,S,R,G,B,M1,M2
        IF (L .LE. .5) THEN
          M2=L*(1+S)
        ELSE
          M2=L+S-L*S
8       END IF
        M1=2*L-M2
        B=rgb_value(M1,M2,H+120)
        R=rgb_value(M1,M2,H)
        G=rgb_value(M1,M2,H-120)
        RETURN
        END


        FUNCTION rgb_value(N1,N2,HUE)
        REAL     rgb_value,N1,N2,HUE
        IF (HUE .GT. 360) THEN
          HUE=HUE-360
        END IF
        IF (HUE .LT. 0) THEN
          HUE=HUE+360
        END IF
        IF (HUE .LT. 60) THEN
          rgb_value=N1+(N2-N1)*HUE/60
        ELSE IF (HUE .LT. 180) THEN
          rgb_value=N2
        ELSE IF (HUE .LT. 240) THEN
          rgb_value=N1+(N2-N1)*(240-HUE)/60
        ELSE
          rgb_value=N1
        END IF
        RETURN
        END

CCCCCCCCCCCCCCCCCCCCCCCCCCCCCCCCCCCCCCCCCCCCCCCCCCCCCCCCCCCCCCCCCCCCCCCCCCC
C       THIS ROUTINE FINDS THE MAX., AND MIN. OF A 100*100 ARRAY
CCCCCCCCCCCCCCCCCCCCCCCCCCCCCCCCCCCCCCCCCCCCCCCCCCCCCCCCCCCCCCCCCCCCCCCCCCC
C
C

        SUBROUTINE SEARCH(ARRAY,AMAX,AMIN)
        DIMENSION ARRAY(100,100)
        AMAX=-1000
        AMIN=1000
        DO 1 I=1,100
            DO 1 J=1,100
```

```
                IF(ARRAY(I,J).GT.AMAX)AMAX=ARRAY(I,J)
                IF(ARRAY(I,J).LT.AMIN)AMIN=ARRAY(I,J)
1       CONTINUE
        RETURN
        END

cccccccccccccccccccccccccccccccccccccccccccccccccccccccccccccccccccccccccccccc
C       THIS ROUTINE CALCULATES THE DIVISIONS ON THE AXES
cccccccccccccccccccccccccccccccccccccccccccccccccccccccccccccccccccccccccccccc
C
C
        SUBROUTINE MARKS(IMGSZ,PER,COORD)
        DIMENSION COORD(5)
        SIZE=PER*IMGSZ/4096.
        COORD(1)=SIZE/-2.
        COORD(2)=SIZE/-4.
        COORD(3)=0
        COORD(4)=SIZE/4.
        COORD(5)=SIZE/2.
        RETURN
        END
```

END

DATE

FILMED

DTIC

4/88